3-2018

Evaluation of Nocturnal Convective Precipitation Over the Great Plains Using Reanalysis Data and a WRF-Based Regional Climate Model

Xu Deng
University of Nebraska-Lincoln, xdeng@huskers.unl.edu

EVALUATION OF NOCTURNAL CONVECTIVE PRECIPITATION OVER THE GREAT PLAINS USING REANALYSIS DATA AND A WRF-BASED REGIONAL CLIMATE MODEL

by

Xu Deng

A THESIS

Presented to the Faculty of

The Graduate College at the University of Nebraska

In Partial Fulfillment of Requirements

For the Degree of Master of Science

Major: Earth and Atmospheric Sciences

Under the Supervision of Professor Qi (Steve) Hu

Lincoln, Nebraska

March, 2018

EVALUATION OF NOCTURNAL CONVECTIVE PRECIPITATION OVER THE GREAT PLAINS USING REANALYSIS DATA AND A WRF-BASED REGIONAL CLIMATE MODEL

Xu Deng, M.S.

University of Nebraska, 2018

Advisor: Qi (Steve) Hu

This study aims to analyze what processes are mainly responsible for nocturnal convective precipitation during the 1991-2000 period for May-June-July over the Great Plains. Firstly, based on the Weather Research and Forecasting model (WRF) coupled with the NCAR Community Land Model (CLM) and the North American Regional Reanalysis (NARR) reanalysis data, the simulations of the diurnal cycles of LLJ and the convective precipitation are examined. Then, the LLJ-related moisture transport is evaluated since the moisture supply is critical for the development of the heavy rainfall. Results show that the WRF model fails to simulate the nocturnal peak rainfall shown in the reanalysis data. The failure in simulating nocturnal maximum precipitation is related to the bias occurring in the modeled nighttime moisture flux divergence/convergence, which suggests that the nocturnal peak convective precipitation may the result of the large-scale processes.

To further figure out the mechanisms controlling the nighttime convection, based on the composite analysis, three 10-case groups are classified: (a) cases that the WRF cannot simulate the timing of the nocturnal peak convective precipitation; (b) cases that the timing of the nocturnal maximum rainfall can be simulated in the model; (c) cases that the maximum precipitation is shown during the afternoon hours in both the NARR data and the WRF model. The comparisons among the three groups suggest that the suppression of daytime convective precipitation and the favoring of nighttime convective precipitation over the Great Plains is closely related to the diurnal cycle of zonal circulation, which is induced by the mountain-plain baroclinic instability. In addition, during nighttime, the intensified anomalous southerly wind, together with the southward forcing above, may have a positive effect on the maintenance of the mountain-plain circulation.

Acknowledgements

I would like to thank my advisor, Dr. Qi (Steve) Hu, for giving me assistance and professional guidance, and my committee members, Dr. Mike Hayes and Dr. Matthew Van Den Broeke, for providing me insightful feedback and incisive comments. I would also like to acknowledge Abraham Torres-Alavez for assisting me with troubleshooting my code and sharing his experience when dealing with problems.

This work would not have been feasible without the funding support by the National Science Foundation (Grant AGS-1355916). I am grateful to the high-performance computing support from the Holland Computing Center at University of Nebraska–Lincoln and Yellowstone (ark:/85065/d7wd3xhc) provided by NCAR's Computational and Information Systems Laboratory, sponsored by the National Science Foundation.

Table of Contents

Chapter 1. Introduction

During the warm season (April–September), the central United States, typically consisting of North Dakota, South Dakota, Nebraska, Kansas, Oklahoma, Texas, Minnesota, Iowa, Missouri, Arkansas, Louisiana, Wisconsin, and Illinois, is characterized by the frequent occurrence of the nocturnal low-level jet (LLJ; Izumi and Barad 1963; Hoecker 1963, 1965; Bonner 1968; Mitchell et al. 1995). In this region, there also exists pronounced precipitation at night, much of which is formed by the deep convection. (e.g., Kincer 1916; Palmen and Newton 1969; Wallace 1975). The relationship between the LLJ and nocturnal maximum rainfall has been widely documented, but are still not well understood (e.g., Means 1952, 1954; Pitchford and London 1962; Higgins 1997; Shapiro et al. 2016). Figuring out the relationship between them and the mechanisms for the formation of the nocturnal peak precipitation can improve the performance of numerical models in the Great Plains. Currently, though the LLJ is simulated quite well, skills on forecasting the nocturnal maximum in rainfall need further improvement.

The LLJ, as the name implies, is a fast-flowing air current typically found in the lower part of the troposphere. There are mainly two classifications of the LLJ, the mid-latitude cyclone induced LLJ and the nocturnal LLJ. For the Great Plains, the latter one is the dominant type and often exhibits a southerly flow. Within the Continental U.S., the LLJ from the Gulf of Mexico is considered to be a major source of moisture supply (Helfand and Schubert 1995; Higgins et al. 1997). Bonner (1968) found that the strength of the diurnal cycle of the LLJ in the warm season (April–September) is stronger than the cold

season (October – March), which is typically in the area of 25–45°N, 90–105°W (Pu and Dickinson 2014). Under the cloud-free and dry atmosphere, surface cooling usually makes it develop in the late afternoon and achieve maximum intensity around midnight. Then after sunrise, the density of turbulence in the planetary boundary layer (PBL) becomes increasingly strong and the LLJ vanishes. During the process, it can bring warm, moist air from the Gulf of Mexico into the continental U.S.

Previous studies have suggested that the formation of the LLJ may be attributed to the following theories. Blackadar (1957) held that the nocturnal LLJ is caused by the inertial oscillation of ageostrophic wind. Due to the surface cooling in the late afternoon, the turbulence in the PBL diminishes, making the daytime balance among the horizontal pressure gradient force, Coriolis force and frictional force (induced by turbulence) break up, finally accelerating air parcels. Holton (1961) showed that the frequent occurrence of the nocturnal LLJ in the Great Plains is the result of pressure gradient force caused by the terrain-related baroclinicity. The above two theories both underline the effects of the PBL. In addition, Wexler (1961) proposed that the topography of North American Cordillera blocks the trade wind from the East and channel the wind northward. Synoptic-scale systems like cold fronts are also conductive to the development of the nocturnal LLJ (Whiteman et al. 1997). Though the mechanism offered by Blackadar (1957) is the most prominent, the nocturnal LLJ may be the result of a combination of the theories.

Over the Great Plains, precipitation exhibits a strong seasonal and diurnal cycle. Not only does the seasonal distribution show a maximum rainfall during the warm season (e.g., Boyle 1998; Wang and Chen 2009), but the diurnal cycle in this period is most significant as well, producing much more rainfall during the nighttime (typically from 0500 – 0800 UTC) than the daytime (e.g., Kincer 1916; Palmen and Newton 1969; Wallace 1975; Dai et al. 1999; Carbone et al. 2002; Carbone and Tuttle 2008). Since most of the nocturnal precipitation is caused by mesoscale convection (e.g. Maddox 1980; Fritsch et al. 1986), convective precipitation, rather than stratiform precipitation, is the main objective in this study. To figure out how the convection occurs, Carbone and Tuttle (2008) summarized that there may mainly be three favorable factors: 1) the eastward-propagating convective episodes cause the convection near the leeside of the Continental Divide and the wave-like (such as gravity wave) mechanisms may result in the propagation velocity; 2) due to the elevated topography of the Rocky Mountains, there is an oscillation of the mountain-plains circulation and ascent movement over the central U.S.; 3) the LLJ transports moist and warm air, producing the moisture convergence.

Since the nocturnal maximum convective precipitation frequently occurs when there exists a nocturnal LLJ (e.g., Bonner 1968; Maddox 1983; Arritt et al. 1997; Tuttle and Davis 2006), how the LLJ relates to the nocturnal peak rainfall has received considerable attention for several decades. Trier and Parsons (1993) conducted a case study over the southern Great Plains, showing that the LLJ can make the environment unstable by transporting warm and moist air. Wilson and Roberts (2006) further pointed out that the coexistence of a stable boundary layer (SBL) and LLJ makes elevated convection (EL)

more likely to happen. The convergence zone is above SBL with the existence of instability.

Although the simulation of LLJ is robust, most numerical models, especially general circulation models (GCMs), still perform relatively low skills in simulating the diurnal cycle of precipitation over the Great Plains, which produce much less precipitation during nighttime than in the daytime (e.g., Ghan et al. 1996; Dai and Trenberth 2004; Demott et al. 2007; Surcel et al. 2010; Pritchard et al 2011). There must be fundamental deficiencies in the structure of the physics parametrization, in which the vital problem lies in the deep convection scheme (e.g., Xie and Zhang 2000; Zhang 2003). Currently, most cumulus schemes employ convective available potential energy (CAPE) as the closure, meaning that the consumption of the deep convection is based on CAPE. As a result, the diurnal cycle of simulated convective precipitation is roughly in phase with the CAPE variation, while the actual situation is that their trends are out of phase (e.g., Dai et al. 1999; Zhang 2003; Demott et al. 2007). Due to the surface cooling, the turbulence in the PBL is reduced, convective inhibition (CIN) increases and the CAPE is much smaller than during the daytime. The resulting large negative buoyancy below the level of free convection (LFC) makes it difficult for the nocturnal deep convection to develop in the model (Kain and Fritsch 1992). Lee et al. (2007) suggested that CAPE is too sensitive to the PBL forcing and there should include dynamical controls on regulating the convection in the scheme, such as the low-level convergence. Furthermore, Lee et al. (2010) noted that the cloud-radiation interaction and middle-level convection should be parametrized into the model. Due to the cloud-top cooling and cloud-base warming, the

atmospheric longwave cooling destabilizes the vertical stability. With the assistance of large-scale vertical moisture advection, the nocturnal convection occurs, of which the mechanism is similar to the convection in the tropical ocean.

This study aims to evaluate the performance of the high-resolution WRF regional climate model to simulate the LLJ and the convective precipitation in the Great Plains, figuring out the processes in the model that are responsible for the simulated biases, which can be used to discuss the mechanisms on how the nocturnal peak precipitation develops and its relationship to the LLJ. In Chapter 2, the simulation configuration and the observed data are described, as well as the methods. Chapter 3 shows the comparisons between the simulated and the reanalyzed data, based on the analysis of 10-year climatology and the composite method. A summary and discussions are provided in Chapter 4.

Chapter 2. Data and Methods

2.1 Reanalysis Data

Ten years (1991–2000) of the National Centers for Environmental Prediction (NCEP) North American Regional Reanalysis (NARR) data (available at http://www.esrl.noaa.gov/psd/) are used to validate the simulation. Furthermore, initial and lateral boundary conditions of the WRF model are also derived from the dataset.

The NARR data is an upgrade of the NCEP Global Reanalysis with higher resolution for the North American continent (Mesinger et al. 2006). Based on the NCEP Eta Model and the Regional Data Assimilation System, the NARR includes a collection of data recorded 8 times a day at 29 vertical levels, from 1000 to 100hPa. There are 349×277 grid points defined on a Lambert Conformal Conic map projection. The horizontal resolution of the dataset is 32 km (approximately 0.3 degrees at the lowest latitude). Since the NARR data assimilates surface rain gauge observations, the precipitation field agrees well with the actual observations, though extreme precipitation is likely underestimated (Mesinger et al. 2006; Sun et al. 2016). Other fields, such as horizontal winds, humidity, temperature and pressure, show significant improvement as well (Jiang et al. 2007; Lee et al. 2007). Berg et al. (2015) also noted that the NARR data can reasonably describe the structure of southerly low-level jet (LLJ) and the patterns of moisture convergence/divergence in the central U.S. However, the frequency of occurrence of the LLJ and its contribution to the total moisture transport are diminished.

2.2 Model Configuration

The simulation by the WRF model (version 3.6) coupled with the NCAR Community Land Model (CLM, version 4.0) was acquired as a product of an NSF funded project (Grant AGS-1355916) on "Quantifying the Relative Roles of Progressive Land Use Change, Irrigation, and Remote Forcing in Southern Great Plains Precipitation Variability". Though the WRF model was not intentionally developed for climate modeling, it has been successfully used for regional climate simulations in the recent decade (Wang and Yang 2008; Caldwell et al. 2009; Zhang et al. 2009; Druyan et al. 2009; Tulich et al. 2011; Sun et al. 2016). For the CLM, more detailed vegetation and hydrological processes are included, such as interactive vegetation canopy and multilayer snow (Cai et al. 2014).

The experiments by the WRF-based regional climate model were carried out in two nested domains (Fig. 1). The outer domain covers approximately from 140−60°W and 23−51°N at a 12-km horizontal resolution (containing 398×284 grid points), and the inner domain is approximately from 85−110°W and 29.8−43.6°N at a 4-km horizontal resolution (containing 451×385 grid points). The model extends vertically from the surface up to 100hPa in 29 hybrid sigma-pressure levels. Physical parameterization schemes used in the model are the Kain−Fritsch scheme describing convection (Kain and Fritsch 1990), the Single-Moment 5-class scheme for cloud microphysics (Hong et al. 2004), YSU scheme for the planetary boundary layer (Hong et al. 2006), and Dudhia

(Dudhia 1989) and Rapid Radiative Transfer Model (Mlawer et al. 1997) (RRTM) schemes for shortwave and longwave radiation transfer, respectively.

It is noted that although the 4-km horizontal resolution in the model inner domain is considered as a convection-permitting resolution (e.g., Weisman et al. 1997; Kain et al. 2008), the assumption that convection can be explicitly resolved by the non-hydrostatic vertical momentum equation at such resolution remains to be further tested (e.g., Bryan et al. 2003; Deng and Stauffer 2006; Gerard 2015). Previous studies have shown that within the range of 1−5km horizontal resolution, employing a convection parameterization scheme decreased a model's prediction skills, e.g., the overlapping of the parameterized and directly resolved convective precipitation (Kuo et al. 1997; Gerard 2007; Gerard et al. 2009; Mahoney 2016; Lind et al. 2016). However, there are still benefits for using convection parameterization in models of such high resolution. Mahoney et al. (2013) suggested that it is helpful to avoid unrealistic accumulation of CAPE when convection parameterization is used. Cintineo et al. (2014) showed that without a convection scheme, it is not sufficient to represent moist convection only based on the microphysics parameterization. Lackmann (2011) pointed out that some fake stratus cloud cover resulted from the absence of a shallow mixing component formulated in the parameterized convection. On the other hand, coarse resolution models that rely on convection schemes often produce spurious sub-grid scale convective precipitation (Molinari and Dudek 1992; Arakawa and Jung 2011; Zheng et al. 2016). These results suggest that the use of convection schemes in a model of convection-resolving horizontal resolution can show some benefits.

Model simulation from 1991–2000 are used in the current study to aid our effort to understand the role of the LLJ from the Gulf of Mexico and the development of nocturnal convection during summertime (May, June and July) in the Great Plains. More details of these schemes and their suitability for the simulation in the NSF funded project were documented in Van Den Broeke et al. (2017) and Hu et al. (2017).

2.3 Methods

First, the performance of the WRF-based regional climate model in simulating the diurnal cycles of convective precipitation and the LLJ over the Great Plains need to be investigated. As prior studies have shown that the GCMs are able to describe the diurnal cycle of the LLJ but unable to describe the diurnal cycle of convection and precipitation (Ghan et al. 1996; Lee et al. 2007; Demott et al. 2007). This discrepancy raised the concern on any important role of the LLJ in initiation and development of nocturnal convection and precipitation in the U.S. Great Plains.

Because the LLJ is most active in May, June and July (Weaver and Nigam 2008), the LLJ events is identified in those months of 1991–2000 based on Bonner's LLJ criteria. The criteria 1, 2 and 3 are defined as follows: the maximum wind velocity is at least 12, 16 or 20 $m\ s^{-1}$ within 1000hPa and 850hPa, and the minimum wind velocity must be no greater than 6, 8, or 10 $m\ s^{-1}$ between the level of maximum wind speed and 700hPa (Bonner 1968; Whiteman et al. 1997; Marengo et al. 2004). Over the same period, moisture transport to the Great Plains is evaluated in terms of changes in low-level

vertically integrated moisture flux and moisture flux divergence, of which their developments are related the large-scale processes.

After identifying the similarities and differences in the diurnal cycle of convective precipitation, the LLJ and the LLJ-related moisture transport between the model and the NARR, composite analysis is employed to examine and interpret those differences and similarities.

Chapter 3. Results

3.1 10-Year Climatology

3.1.1 Diurnal Cycle of Convective Precipitation

Prior research has shown that many GCMs exhibited a relatively high skill in simulating the LLJ but need further improvement in forecasting nocturnal rainfall (e.g., Ghan et al. 1996; Lee at el. 2007). To compare with those prior studies, the diurnal cycles of convective precipitation by the NARR data and the WRF-based regional climate model are analyzed over the 10-year (1991-2000) period for May-June-July (MJJ).

The diurnal cycle of 3h-accumulated MJJ convective precipitation from the NARR and the WRF are shown in Figs. 2 and 3, respectively. There are clear differences in the simulated and reanalyzed diurnal cycle of convection in the Great Plains. In the NARR, Fig. 2 shows the convective precipitation maximum occurring from 2100-0300 LT in the area from northern Oklahoma to Kansas and Nebraska. The temporal evolution of convection in Fig. 2 suggests that convection occurred in the Great Plains with weak southeastward propagation after peak convection in the midnight hour.

On the contrary, the WRF simulated convection and convective precipitation shown in Fig. 3 have their maximum in the early- to mid-afternoon hours, which is most distinct along the Continental Divide (off to the west of the Great Plains). There is little

convective precipitation in the late night-early morning hours. It suggests that the WRF model, even with a high resolution, still cannot capture the nocturnal peak rainfall over the Great Plains.

3.1.2 Diurnal Cycle of the LLJ

The LLJ events in MJJ of 1991-2000 are identified based on Bonner's LLJ criteria. Figure 4 shows the direction (phase) of the most frequently occurring LLJ (criterion 2) averaged for MJJ of 1991-2000 from the NARR data (Fig. 4a) and from the WRF (Fig. 4b). The vectors pointing to south, west, north and east in Fig. 4 indicate highest frequency of the southerly LLJ occurring at 0000, 0600, 1200 and 1800 LT. Though the model generally simulates nocturnal LLJ events with a larger frequency than that in the NARR data, the result shows that simulated strongest southerly low-level winds occur most often around local midnight hour, consistent with the NARR data.

Some large differences in the diurnal cycle of the low-level winds between the simulated and the reanalysis data are found in the areas where the mountainous terrain meets with the plains in eastern Colorado and Wyoming. In those areas, the maximum LLJ frequency occurs at 0600 LT in the reanalysis data, but it occurs around local noon hour in the WRF. It suggests that the model is still weak in simulating low-level winds in areas of complex terrain. Another difference is in the narrow corridor from southwestern Texas to northeastern Oklahoma where the simulation is approximately 3 hours ahead of that in the NARR data.

Though the simulated LLJ in the Great Plains is relatively consistent with the NARR (Fig 4), compared to the in-phase relationship shown in the NARR (Fig. 2), there is a mismatch between the simulated diurnal cycle of the LLJ and convective precipitation in the Great Plains (Fig 3). The simulation results of the strong LLJ during the nocturnal hours and the absence of simultaneous convective precipitation make it necessary to investigate the role of the LLJ in initiation and development of convection in the nocturnal hours. In the following section, to answer the question why the strong LLJ corresponded with little convection in the nocturnal hours, the LLJ-related moisture transport needs to be first examined.

3.1.3 Diurnal Cycle of Low-Level Moisture Transport

For moderate and heavy precipitation, it is the abundant moisture supply that sustains such events, not directly from evaporation (Trenberth et al. 2003). Since most water vapor is concentrated below 700hPa (Van Zomeren and Van Delden 2007), vertically integrated moisture flux (VIMF) and moisture flux divergence (VIMFD) in the lower troposphere are employed to investigate the impact of LLJ on the moisture transport.

As the direction of the LLJ is usually northward, the low-level VIMF for meridional wind is calculated using the following equation (Torres-Alavez et al. 2014),

$$\text{VIMF} = -\frac{1}{g}\int_{p_s}^{p}(vq)dp \qquad (3.1.1)$$

The low-level VIMFD is defined as follows (Van Zomeren and Van Delden 2007),

$$\text{VIMFD} = -\frac{1}{g}\int_{p_s}^{p}\left(\frac{\partial uq}{\partial x}+\frac{\partial vq}{\partial y}\right)dp \qquad (3.1.2)$$

where u and v represent the zonal and meridional wind velocity respectively, q is the specific humidity, and g is the gravitational acceleration. Both integrations in (3.1.1) and (3.1.2) are calculated between 1000hPa (taken as surface) and 700hPa. The units are $kg\ m^{-1}\ s^{-1}$ for VIMF and $kg\ m^{-2}\ s^{-1}$ for VIMFD.

The temporal and spatial patterns of low-level troposphere VIMF calculated from the NARR data and the WRF both exhibit similar diurnal cycles, with the intensity of northward low-level moisture transport overnight being much larger than that in the daytime (Figs. 5 and 6). The core of the flow is found between 102°W and 92°W. VIMF from the NARR data shows strong nighttime transport persistent for a longer time (0000 to 0600 LT), with the maximum occurring at 0600 LT in the northeast Texas. In comparison, the VIMF calculated from the WRF output is lower than that from the reanalysis data. Along the Rocky Mountains, there appears southward transport in the lower troposphere, which is almost absent in the VIMF calculated from NARR data. In general, the peak intensity of VIMF around the local midnight hour in both these results matches with the peak intensity of the LLJ (Fig 2), indicating a strong contribution of the LLJ to the large VIMF.

Vertically integrated convergence and divergence of moisture in the lower troposphere calculated from equation (3.1.2) using NARR data and the WRF model is shown in Figs. 7 and 8. Convergence (divergence) can cause rising (sinking) motion in the lower troposphere, often being used as an indicator for precipitation development (e.g., Moseley et al. 2016). In Figs. 7 and 8, positive values represent moisture flux divergence

and negative indicate moisture flux convergence.

As shown in Fig. 7, positive VIMFD is observed spreading in the Plains in local afternoon hours, with a narrow strip of convergence in the eastern slope of the Rocky Mountains (1200–1800 LT). It reflects intensification of the uphill winds in the mountain-plain topography. This pattern is reversed after the sunset and persists through the early morning hours (2100–0600 LT), when mountain winds develop from the cool eastern slope of the Rockies. The mountain winds converge over the central and southern Great Plains where the intensifying LLJ brings moisture into the region. Consistent with the development of the mountain winds and related convergence over the Plains, convective precipitation shown in Fig. 2 occurs along the convergence zone, and the rain areas spread slowly toward the mountain hills as the LLJ intensifies in the early morning hours.

For the WRF model (Fig. 8), in the afternoon, the pattern of low-level moisture flux divergence/convergence is similar to that in the NARR data. However, during nighttime, the simulated moisture flux divergence in the lower troposphere along the eastern slope of the Rocky Mountains is not strong enough or organized well. Meanwhile, the convergence in the central Plains is much weaker than that diagnosed from the NARR data. The lack of strong moisture flux convergence in the plains could have contributed to the lack of precipitation from midnight to early morning hours in the model simulation.

Previous studies have suggested that it is the convection schemes that could be responsible for the phase bias in model-simulated diurnal rainfall in the warm season (e.g. Lee et al. 2007; Demott et al. 2007). Most cumulus schemes, including the Kain-Fritsch (KF) scheme, employ CAPE as the measure of vertical instability and the drive for convection. In the following sections, how the convection in the Great Plains varies in relation to the CAPE will be examined in WRF model and in the NARR. And then, the cause of processes for the development of those different convection cases will be identified.

3.2 Composite Analysis

Composite analysis is a useful tool to smooth out the anomalies of individual cases and refine the most prominent dynamic and thermodynamic features. In this study, the philosophy for the analysis is as follows:

1) A domain of 2×2 degrees, covering 37–39˚N and 99–97˚W, is used to select convective precipitation (CP) cases. The study area covers southern Kansas, where there shows a distinct nocturnal maximum in rainfall;
2) When selecting the precipitation cases, a “day” is defined from 1200 LT of the current day to 1200 LT of the following day. In this way, the early morning CP events can be put in the “same day” with the afternoon events that occurred in the previous calendar day.

Since convective precipitation could occur in different times of a day (e.g., afternoon, early evening and early morning hours), based on the above criteria, three groups of CP cases (each containing 10 cases) are categorized during the 1991–2000 period for May–July. The composite results are shown in Fig. 9, in which the solid lines show the precipitation from convective events in the NARR and the dashed lines represent the simulated precipitation. In Group 1, the NARR data shows a strong peak in convective precipitation in the early morning hours (peak at 0300 LT) whereas the simulation results show very weak convective precipitation (weaker than 1/3 of that from the NARR data) in the early afternoon hours (1200–1500 LT). This complete mismatch indicates the model's inability to describe the nocturnal convection and precipitation in this Group.

Composite results in Group 2 are shown in Fig. 9b. Increased convective rainfall in this group begins at 2100 LT and achieves maximum 3 hours later. The model-simulated convection averaged for the same days occurred near the midnight (2100 LT) with a relatively small peak. For these events, the model apparently could describe the timing of convective precipitation as that reported in the NARR data although the intensity is about 1/3 of that in the NARR data.

Composite results for Group 3 are shown in Fig. 9c. Convective precipitation in this group occurred in the early afternoon hours with a peak at 1500 LT in the NARR data and a peak around 1200 LT in the model simulation. Both the phase and the intensity of the simulated convective precipitation are similar to that in the NARR data.

3.2.1 Diurnal Cycle of Convective Precipitation and CAPE

In KF scheme, the convection is largely determined by the amount of CAPE and CIN, which are generally used to measure atmospheric instability in the atmosphere. Moseley et al. (2016) pointed out that CAPE generally intensifies after the occurrence of precipitation and declines with precipitation continuing. Since CAPE (CIN) represents the integral of positive buoyancy (negative buoyancy), they are defined by:

$$\text{CAPE} = \int_{Z_{LFC}}^{Z_{EL}} g\left(\frac{T_{vp}-\overline{T_v}}{\overline{T_v}}\right) dz \qquad (3.2.1)$$

$$\text{CIN} = \int_{Z_{SFC}}^{Z_{LFC}} g\left(\frac{T_{vp}-\overline{T_v}}{\overline{T_v}}\right) dz \qquad (3.2.2)$$

where Z_{LFC} is the height of the level of free convection, $Z_{EL}$is the height of equilibrium level and Z_{SFC} is that of the surface level or the beginning of a parcel path. T_{vp} represents the virtual temperature of the parcel, and $\overline{T_v}$ denotes the virtual temperature of the environment. Zhang (2003) has noted that T_{vp} can be modified by the surface sensible and latent heat while $\overline{T_v}$ can change due to large-scale processes.

The composite of the CAPE and CIN for convection events in each of the three groups are shown in Figs. 9d–f. Compared to the corresponding convective precipitation in Figs. 9a–c, some striking differences are shown between the NARR data and the WRF model.

In Group 1, the convective precipitation in the NARR (Fig. 9a) reaches maximum in the early morning (0300 LT) when the CAPE is near its diurnal minimum and the CIN is relatively large. Yet, the model-simulated peak precipitation in the early afternoon (1500 LT) occurs simultaneously with the maximum CAPE and the minimum CIN shown in the

Fig. 9d. Compared to the simulated results with the reanalysis data, the difference in the relationship between the CAPE and convective rainfall suggests that the KF cumulus scheme used in the WRF model may result in the misrepresentation of diurnal cycle of convective precipitation.

For Group 2, the diurnal variations of the CAPE in both the WRF and the NARR reach maximum at 1800 LT (Fig 9e), which is generally consistent with that of nocturnal precipitation shown in Fig 9b. Though the nocturnal peak rainfall in the WRF occurs 3 hours earlier than that in the NARR, it shows that the model in Group 2 can simulate the timing of the nocturnal convective precipitation relatively well. It is also noted that, compared to the first group, the timing of the maximum CAPE occurs 3 hours later, and its magnitude is much smaller. As Zhang (2003) noted that the CAPE can be influenced either by the PBL forcing or by the large-scale forcing, the closer relationship between the CAPE and nocturnal convective rainfall may suggest that in this group the PBL forcing is less dominant and the large-scale processes are simulated relatively well.

In Group 3, the maximum CAPE in the WRF occurs at the noon hour (1200 LT) and in the NARR data, it occurs at 1500 LT, both of which are consistent with that of convective precipitation in Fig 9c. These convective rainfall events occurred at the time when the CAPE is relatively large and the CIN is relatively weak (Figs. 9c and 9f). It is likely that the convection in afternoon hours in this group is primarily caused by the PBL forcing which can be simulated well by this model (e.g. Dai et al. 1999; Lee et al. 2007; Moseley et al. 2016).

To summarize, three groups of convective precipitation cases in our study region of the Great Plains are identified. In Group 1, the WRF model can simulate neither the timing of nocturnal convective precipitation nor the amount of it. For events in Group 2, though the precipitation intensity in the simulation is still much smaller, the timing of convective precipitation in the model is relatively consistent with the NARR data, which occurs 3 hours before convective precipitation reaches the maximum in the reanalysis data. The convective rainfall in Group 3 exhibits peak intensity in the afternoon in both the WRF and the NARR data. For all three groups, it is noted that the convective precipitation simulated by the WRF model is closely related to the CAPE, which suggests that the CAPE may be inappropriate to be used for simulating nocturnal convection over the Great Plains.

Finding the cause of the model's failure in simulating the nocturnal convective precipitation is beyond the scope of this work. In the next section, the differences in the zonal circulation between the WRF model and the NARR are analyzed for the three groups. Investigating the problem from a different angle, not from the CAPE, would strengthen the understanding of how nocturnal convection develops over the Great Plains and the relationship between the CAPE and nocturnal convective precipitation.

3.2.2 Diurnal Cycle of Zonal Circulation

To figure out what mechanisms induce the different diurnal cycles of convective precipitation in those three groups, the longitudinal cross sections of diurnal anomalies

(from daily mean) of zonal circulation, meridional wind and temperature are examined, which are averaged over 37–39˚N.

Figures 10 and 11 show the cross sections of zonal circulation between the convective precipitation events in Group 1, using the NARR reanalysis data and the WRF model simulation. In Fig. 10, from 1200 to 1500 LT, due to the solar radiation, there is a distinct horizontal temperature gradient in the lower troposphere (below 700hPa) between the mountainous areas and the plains, for which the mountainous areas are relatively warmer. Consequently, the baroclinic instability induced by the temperature gradient produces a clockwise circulation extending from the ground surface to almost 250hPa. The downward branch of the circulation is over the Great Plains and the upward branch is over the mountainous areas, which corresponds to the divergence/convergence pattern in the same period shown in Fig. 7. Meanwhile, the sensible and latent heating intensify, making the boundary layer well mixed. The resulting frictional force in the PBL reduces the meridional wind (anomalous northerly) in the lower levels (below 850hPa), and an anomalous northward wind is shown in the upper levels (above 850hPa) due to the Coriolis force on the westward motion. Together with the low-level moisture convergence over the Rockies, the moisture transported by the anomalous northward wind is favorable for the occurrence of convective precipitation in the afternoon (Fig. 3).

In the late afternoon and evening (1800–2100 LT), since the intensity of solar radiation diminishes, the temperature gradient begins to decrease, making the direction of the zonal circulation reverse and become counterclockwise at 2100 LT. Compared to the conditions

in the afternoon, the downward branch of the circulation changes to be over the Rockies and the upward branch over the Great Plains. Meanwhile, the anomalous southerly wind, induced by the decoupling of nighttime PBL from surface and the thermal wind, represents that the LLJ transports moisture into the Great Plains, which is consistent with the results in Fig. 5. In addition, because of Coriolis effect, the intensified southerly wind, together with the northerly wind above, can make the zonal circulation stronger. As surface cooling continues, the counterclockwise circulation reaches most pronounced at 0000 LT and begin to decay until 0600 LT. During the period (0600 – 0900 LT), the pattern of daytime diurnal anomalies of zonal circulation, meridional wind and temperature start to rebuild.

For the WRF model in Group 1 (Fig. 11), it is difficult to identify a mountain-plain circulation in the simulation results. Although there occurs a clear downward motion over the Rocky Mountains at 0000CST, the zonal vertical motion is less organized over the Great Plains. In addition, the simulation of anomalous northward forcing in the lower levels is also less organized. One possible reason is that the downward motion over the Rockies in simulation is not as strong as in the NARR data after the sunset, especially around midnight. A weaker downward motion over the mountains would have weaker circulation so that the upward forcing to lift warmer and moist air over the Plains is hard to initiate and support the convection.

For Group 2, the diurnal anomalies of the simulated zonal circulation, meridional wind and temperature are more comparable to the NARR data (Figs. 12 and 13) than that in

Group 1. Similar to the Fig. 10, the NARR data shows a clockwise circulation in the afternoon hours (1500–1800 LT), and a reversed counterclockwise circulation in nocturnal hours (2100–0300 LT). In contrast, though less pronounced than that in the NARR (Fig. 12), the temporal and spatial patterns of anomalous zonal circulation and meridional wind are simulated relatively well (Fig. 13). By comparing the NARR with the WRF model in Group 2, it suggests that the weaker zonal circulation shown in the WRF may be one of the possible reasons that result in the smaller intensity of precipitation (Fig. 9b).

In Group 3, it is the only group with more modeled convective precipitation than that reported in NARR data. For the NARR, though the overall pattern of zonal circulation is similar to that in the Groups 1 and 2, the structure of the circulation in the reanalysis data is a lot weaker (Fig. 14), which may reduce the suppression/favoring effect on convection over the plains in the afternoon/midnight. In this way, the PBL forcing can overcome the suppression and induce peak rainfall at 1500 LT in the domain (99–97˚W, 37–39˚N) for composite analysis. And the nocturnal maximum convective precipitation is hard to produce during the nighttime (0000–0300 LT). In WRF model, over the Great Plains, the simulated zonal circulation (Fig. 15) can facilitate/suppress the occurrence of convective precipitation in the afternoon/night, which is similar to Group 1 (Fig. 11).

To summarize, the three groups of cases are used to calculate the longitudinal cross sections of diurnal variations of zonal circulation, meridional wind and temperature, which can strengthen the understanding of how the nocturnal convective precipitation

develops. For the NARR data, in Groups 1 and 2, the suppression of daytime convective rainfall over the Great Plains is due to the down-branch of the clockwise solenoid circulation. In contrast, maximum convective precipitation over the Plains occurred around the midnight and has an in-phase relationship with the establishment of the counterclockwise solenoidal circulation, which has a deep layer of upward motion over the Great Plains. In Group 3, due to the weaker structure of zonal circulation, the PBL forcing can overcome the suppression of the down-branch of the clockwise circulation and produce rainfall with a relative small intensity. As shown in Figs 16–18, which respectively show east-west-oriented cross sections of diurnal cycles of vertical velocity, relative humidity and isentropes averaged between 37°N and 39°N for Groups 1–3, the diurnal cycles of vertical velocity are consistent with the diurnal deviations of zonal vertical circulation, further suggesting that the solenoid circulation is closely related to the suppression/inducement of convection over the Great Plains.

For the WRF model, in Groups 1 and 3, the diurnal cycles of anomalous zonal circulation are not well simulated. It may be due to the fact that the model employs the CAPE to assess the likelihood of convection and the CAPE usually reaches maximum mostly because of the sensible and latent heating. In contrast, the CAPE in the Group 2 reaches maximum later than the other two groups, suggesting that the large-scale processes (e.g. the mountain-plain solenoidal circulation) may be more significant. For more mechanically induced convection without substantial amount of CAPE involved, the model may have difficulty in recognizing the large-scale processes. Moreover, the intensity of the simulated nighttime convective rainfall is much smaller compared to the

NARR data. One possible reason is that the model does not take the moisture transported by the LLJ into consideration. A lager domain (4˚×4˚) for the composite analysis, covering 36–40˚N and 100–96˚W, has also been analyzed (not shown). The results shown in the NARR data also shows similar diurnal cycles of zonal circulation and vertical velocity, further strengthening the conclusion.

Consistent with previous studies (Carbone and Tuttle 2008; Sun et al. 2016), the mountain-plain circulation is shown in the NARR data for all the three groups. Sun et al. (2016) also found that the anomalous zonal circulation was simulated relatively well based on May-through-August averages for 10 years (2000–2009). However, in this study, there are no similar diurnal cycles of zonal circulation for the simulation in Groups 1 and 3, One possible reason is that they averaged the fields for a larger latitudinal range (30–40˚N), which would smooth out the distinct features for convective systems.

Chapter 4. Discussion and Conclusion

Based on the WRF-based regional climate model and the NARR data, this study aims to evaluate its performance in simulating the nocturnal peak convective precipitation and try to figure out the mechanisms for its development during the 1991-2000 period for May-June-July over the Great Plains. Previous studies have shown that fields like temperature, LLJ, moisture transport, wind fields etc. are realistic in the NARR data, which can be used as the verification (e.g. Jiang et al. 2007; Lee et al. 2007; Sun et al. 2016).

The LLJ is widely considered to be an important factor in the formation of the nocturnal convection. Though the high-resolution (4km) model can simulate the amplitude and phase of maximum LLJ frequency, it fails to describe the nocturnal peak rainfall. Furthermore, LLJ-related moisture transport is examined. Though the smaller intensity, the diurnal cycle of the simulated VIMF is generally consistent with that in the NARR. However, the simulation of the VIMFD shows that the simulated low-level moisture flux divergence along the eastern slope of the Rocky Mountains is not organized well and the convergence over the Plains is relatively weak. It suggests that the nocturnal maximum convective precipitation is related to large-scale processes.

In order to identify the above discrepancies, three groups of 10-case composites are defined as follows: (a) cases that the WRF cannot capture the timing of nocturnal peak convective precipitation; (b) cases that the model can simulate the timing of nocturnal rainfall; (c) cases that there shows peak convective precipitation during afternoon hours in both the WRF and the NARR. Since the deep convection is closely related the amount

of CAPE in the WRF model, the simulation of the peak convective precipitation occurs in the afternoon for both the Groups 1 and 3. However, for the nocturnal maximum convective precipitation in Groups 1 and 2, it shows a relatively closer relationship between CAPE and rainfall in the model and the reanalysis data. Since the CAPE is related to either the PBL forcing or the large-scale processes (Zhang 2003), the CAPE in these events may be more related to the large-scale processes.

Through the longitudinal cross sections of diurnal variations of the anomalous zonal vertical circulation and the vertical velocity, the interaction between large-scale forcing and PBL forcing is further investigated. Since in the afternoon the downward large-scale forcing (baroclinic instability) is usually larger than the upward PBL forcing (sensible and latent heating), the daytime convection in central U.S. is often suppressed below 500hPa. While at night, though the shutdown of solar radiation, the net effect of upward forcing by the mountain-plain baroclinic instability favors the development of nocturnal rainfall. In addition, the LLJ not only transports a large amount of warm and moist air, but also may have a positive effect on the structure of mountain-plain circulation.

One concern on nocturnal convection is the elevated convection, which is considered to explain how the nighttime convection is maintained with the occurrence of the LLJ and a stable boundary layer (e.g. Reif and Bluestein 2017; Blake et al. 2017; Trier et al. 2017). As shown in Fig. 19a, the acceleration of the vertical velocity from 925hPa to 850hPa is suppressed when the surface cooling occurs (0000 LT), while the velocity in upper levels (500hPa and 300hPa) increases a lot, indicating that the deep convection begins to

develop above the PBL, not the typical near-surface layer. For the Group 2 (Fig. 19b), the diurnal cycle of vertical motion is similar to Group 1, though the timing for intensified upper-level vertical motion is 3 hours earlier. Compared to Groups 1 and 2, there is no nighttime upper-level vertical motion shown in Group 3 (Fig. 19c), which is consistent with the diurnal cycle of rainfall in Fig. 9c.

In the future, the mechanisms suggested in this study will be tested by the model experiments and verified by more observational cases. Since there are different convective modes, which have different locations, wind profile and etc., the relationship between the zonal circulation and convective modes can be analyzed in the meantime. More details on how the mountain-plain solenoidal circulation is favorable for the initiation and development of the elevated convection should also be further examined. Besides the cumulus scheme, model parameterizations like the PBL scheme and microphysics are also significant in resolving the large-scale forcing and should be analyzed and modified.

References

Arakawa, A., and J.-H. Jung, 2011: Multiscale modeling of the moist convective atmosphere—A review. *Atmospheric Research*, **102,** 263–285.

Arritt, R. W., T. D. Rink, M. Segal, D. P. Todey, C. A. Clark, M. J. Mitchell, and K. M. Labas, 1997: The Great Plains low-level jet during the warm season of 1993. *Monthly Weather Review*, **125,** 2176–2192.

Berg, L. K., L. D. Riihimaki, Y. Qian, H. Yan, and M. Huang, 2015: The low-level jet over the southern Great Plains determined from observations and reanalyses and its impact on moisture transport. *Journal of Climate*, **28,** 6682–6706.

Blackadar, A. K., 1957: Boundary layer wind maxima and their significance for the growth of nocturnal inversions. *Bulletin of the American Meteorological Society*, **38,** 283–290.

Blake, B. T., D. B. Parsons, K. R. Haghi, and S. G. Castleberry, 2017: The structure, evolution, and dynamics of a nocturnal convective system simulated using the WRF-ARW model. *Monthly Weather Review*, **145,** 3179–3201.

Bonner, W. D., 1968: Climatology of the low-level jet. *Monthly Weather Review*, **96,** 833–850.

Boyle, J. S., 1998: Evaluation of the annual cycle of precipitation over the United States in GCMs: AMIP simulations. *Journal of Climate*, **11,** 1041–1055.

Bryan, G. H., J. C. Wyngaard, and J. M. Fritsch, 2003: Resolution requirements for the simulation of deep moist convection. *Monthly Weather Review*, **131,** 2394–2416.

Cai, X., Z.-L. Yang, Y. Xia, M. Huang, H. Wei, L. R. Leung, and M. B. Ek, 2014: Assessment of simulated water balance from Noah, Noah-MP, CLM, and VIC over CONUS using the NLDAS test bed. *Journal of Geophysical Research: Atmospheres*, **119,** 13751–13770.

Caldwell, P., H.-N. S. Chin, D. C. Bader, and G. Bala, 2009: Evaluation of a WRF dynamical downscaling simulation over California. *Climatic Change*, **95,** 499–521.

Carbone, R. E., J. D. Tuttle, D. A. Ahijevych, and S. B. Trier, 2002: Inferences of predictability associated with warm season precipitation episodes. *Journal of the Atmospheric Sciences*, **59,** 2033–2056.

Carbone, R. E., and J. D. Tuttle, 2008: Rainfall occurrence in the U.S. warm season: The diurnal cycle. *Journal of Climate*, **21,** 4132–4146.

Cintineo, R., J. A. Otkin, M. Xue, and F. Kong, 2014: Evaluating the performance of planetary boundary layer and cloud microphysical parameterization schemes in convection-permitting ensemble forecasts using synthetic GOES-13 satellite observations. *Monthly Weather Review*, **142,** 163–182.

Dai, A. G., and C. Deser, 1999: Diurnal and semidiurnal variations in global surface wind and divergence fields. *Journal of Geophysical Research: Atmospheres*, **104,** 31109–31125.

Dai, A., and K. E. Trenberth, 2004: The diurnal cycle and its depiction in the Community Climate System Model. *Journal of Climate*, **17,** 930–951.

Demott, C. A., D. A. Randall, and M. Khairoutdinov, 2007: Convective precipitation variability as a tool for general circulation model analysis. *Journal of Climate*, **20,** 91–112.

Deng, A., and D. R. Stauffer, 2006: On improving 4-km mesoscale model simulations. *Journal of Applied Meteorology and Climatology*, **45,** 361–381.

Druyan, L. M., M. Fulakeza, P. Lonergan, and E. Noble, 2009: Regional climate model simulation of the AMMA Special Observing Period #3 and the pre-Helene easterly wave. *Meteorology and Atmospheric Physics*, **105,** 191–210.

Dudhia, J., 1989: Numerical study of convection observed during the Winter Monsoon Experiment using a mesoscale two-dimensional model. *Journal of the Atmospheric Sciences*, **46,** 3077–3107.

Fritsch, J. M., R. J. Kane, and C. R. Chelius, 1986: The contribution of mesoscale convective weather systems to the warm-season precipitation in the United States. *Journal of Climate and Applied Meteorology*, **25,** 1333–1345.

Gerard, L., 2007: An integrated package for subgrid convection, clouds and precipitation compatible with meso-gamma scales. *Quarterly Journal of the Royal Meteorological Society*, **133,** 711–730.

Gerard, L, J.-M. Piriou, R. Brožková, J.-F. Geleyn, and D. Banciu, 2009: Cloud and precipitation parameterization in a meso-gamma-scale operational weather prediction model. *Monthly Weather Review*, **137,** 3960–3977.

Gerard, L., 2015: Bulk mass-flux perturbation formulation for a unified approach of deep convection at high resolution. *Monthly Weather Review*, **143,** 4038–4063.

Ghan, S. J., X. Bian, and L. Corsetti, 1996: Simulation of the Great Plains low-level jet and associated clouds by general circulation models. *Monthly Weather Review*, **124,** 1388–1408.

Helfand, H. M., and S. D. Schubert, 1995: Climatology of the simulated Great-Plains low-level jet and its contribution to the continental moisture budget of the United States. *Journal of Climate*, **8,** 784–806.

Higgins, R. W., Y. Yao, E. S. Yarosh, J. E. Janowiak, and K. C. Mo, 1997: Influence of the Great Plains low-level jet on summertime precipitation and moisture transport over the central United States. *Journal of Climate*, **10,** 481–507.

Hoecker, W. J., 1963: Three southerly low-level jet systems delineated by the Weather Bureau special pibal network of 1961. *Monthly Weather Review*, **91,** 573–582.

Hoecker, W. J., 1965: Comparative physical behavior of southerly boundary layer jets. *Monthly Weather Review*, **93,** 133–144.

Holton, J. R., 1967: The diurnal boundary layer wind oscillation above sloping terrain. *Tellus*, **19,** 199–205.

Hong, S. Y., J. Dudhia, and S. H. Chen, 2004: A revised approach to ice microphysical processes for the bulk parameterization of clouds and precipitation. *Monthly Weather Review*, **132,** 103–120.

Hong, S. Y., Y. Noh, and J. Dudhia, 2006: A new vertical diffusion package with an explicit treatment of entrainment processes. *Monthly Weather Review*, **134,** 2318–2341.

Hu, Q., J. A. Torres-Alavez and M. S. Van Den Broeke, 2017: Land-cover change and the "Dust Bowl" drought in the U.S. Great Plains. Submitted to *Journal of Climate*.

Izumi, Y., and M. L. Barad, 1963: Wind and temperature variations during development of a low-level jet. *Journal of Applied Meteorology*, **2,** 668–673.

Jiang, X., N. C. Lau, I. M. Held, and J. J. Ploshay, 2007: Mechanisms of the Great Plains low-level jet as simulated in an AGCM. *Journal of the Atmospheric Sciences*, **64,** 532–547.

Kain, J. S., and J. M. Fritsch, 1990: A one-dimensional entraining/detraining plume model and its application in convective parameterization. *Journal of the Atmospheric Sciences*, **47,** 2784–2802.

Kain, J. S., and J. M. Fritsch, 1992: The role of the convective "trigger function" in numerical forecasts of mesoscale convective systems. *Meteorology and Atmospheric Physics*, **49,** 93–106.

Kain, J. S., and Coauthors, 2008: Some practical considerations regarding horizontal resolution in the first generation of operational convection-allowing NWP. *Weather and Forecasting*, **23,** 931–952.

Kincer, J. B., 1916: Daytime and nighttime precipitation and their economic significance. *Monthly Weather Review*, **44,** 628–633.

Kuo, Y. H., J. Bresch, M.-D. Cheng, J. Kain, D. B. Parsons, W.-K. Tao, and D.-L. Zhang, 1997: Summary of a mini-workshop on cumulus parameterization for mesoscale models. *Bulletin of the American Meteorological Society*, **78,** 475–491.

Lackmann, G. M., 2011: *Midlatitude Synoptic Meteorology: Dynamics, Analysis, and Forecasting*. American Meteorology Society, 345 pp.

Lee, M.-I., S.D. Schubert, M.J. Suarez, I.M. Held, N. Lau, J.J. Ploshay, A. Kumar, H. Kim, and J.E. Schemm, 2007: An analysis of the warm season diurnal cycle over the continental United States and northern Mexico in general circulation models. *Journal of Hydrometeorology*, **8,** 344–366.

Lee, M.-I., I. Choi, W.-K. Tao, S. D. Schubert, and I.-S. Kang, 2010: Mechanisms of diurnal precipitation over the U.S. Great Plains: A cloud resolving model perspective. *Climate Dynamics*, **34,** 419–437.

Lind, P., D. Lindstedt, E. Kjellström, and C. Jones, 2016: Spatial and temporal characteristics of summer precipitation over Central Europe in a suite of high-resolution climate models. *Journal of Climate*, **29,** 3501–3518.

Maddox, R. A., 1980: Mesoscale convective complexes. *Bulletin of the American Meteorological Society*, **61,** 1374–1387.

Mahoney, K. M., M. Alexander, J. D. Scott, and J. Barsugli, 2013: High-resolution downscaled simulations of warm-season extreme precipitation events in the Colorado Front Range under past and future climates. *Journal of Climate*, **26,** 8671–8689.

Mahoney, K. M., 2016: The representation of cumulus convection in high-resolution simulations of the 2013 Colorado Front Range flood. *Monthly Weather Review*, **144,** 4265–4278.

Marengo, J. A., W. R. Soares, C. Saulo, and M. Nicolini, 2004: Climatology of the low-level jet east of the Andes as derived from the NCEP–NCAR reanalyses: Characteristics and temporal variability. *Journal of Climate*, **17,** 2261–2280.

Means, L. L., 1952: On thunderstorm forecasting in the central United States. *Monthly Weather Review*, **80,** 165–189.

Means, L. L., 1954: A study of the mean southerly wind-maximum in low levels associated with a period of summer precipitation in the Middle West. *Bulletin of the American Meteorological Society*, **35,** 166–170.

Mesinger, F., and Coauthors, 2006: North American regional reanalysis. *Bulletin of the American Meteorological Society*, **87,** 343–360.

Mitchell, M. J., R. A. Arritt, and K. Labas, 1995: A climatology of the warm season Great Plains low-level jet using wind profiler observations. *Weather and Forecasting*, **10,** 576–591.

Mlawer, E. J., S. J. Taubman, P. D. Brown, M. J. Iacono, and S. A. Clough, 1997: Radiative transfer for inhomogeneous atmospheres: RRTM, a validated correlated-k model for the longwave. *Journal of Geophysical Research: Atmospheres*, **102,** 16663–16682.

Molinari, J., and M. Dudek, 1992: Parameterization of convective precipitation in mesoscale numerical models: A critical review. *Monthly Weather Review*, **120,** 326–344.

Moseley, C., C. Hohenegger, P. Berg, and J. O. Haerter, 2016: Intensification of convective extremes driven by cloud-cloud interaction. *Nature Geoscience*, **9,** 748–752.

Palmen, E., and C. W. Newton, 1969: *Atmospheric Circulation Systems: Their Structure and Physical Interpretation*. Academic Press, 292–294.

Pitchford, K. L., and J. London, 1962: The low-level jet as related to nocturnal thunderstorms over Midwest United States. *Journal of Applied Meteorology*, **1,** 43–47.

Pritchard, M. S., M. W. Moncrieff, and R. C. J. Somerville, 2011: Orogenic propagating precipitation systems over the United States in a global climate model with embedded explicit convection. *Journal of the Atmospheric Sciences*, **68,** 1821–1840.

Pu, B., and R. E. Dickinson, 2014: Diurnal spatial variability of Great Plains summer precipitation related to the dynamics of the low-level jet. *Journal of the Atmospheric Sciences*, **71,** 1807–1817.

Reif, D. W., and H. B. Bluestein, 2017: A 20-year climatology of nocturnal convection initiation over the Central and Southern Great Plains during the warm season. *Monthly Weather Review*, **145,** 1615–1639.

Shapiro, A., E. Fedorovich, and S. Rahimi, 2016: A unified theory for the Great Plains nocturnal low-level jet. *Journal of the Atmospheric Sciences*, **73,** 3037–3057.

Sun, X., M. Xue, J. Brotzge, R. A. McPherson, X. M. Hu, and X. Q. Yang, 2016: An evaluation of dynamical downscaling of central plains summer precipitation using a WRF-based regional climate model at a convection-permitting 4km resolution. *Journal of Geophysical Research: Atmospheres*, **121,** 13801–13825.

Surcel, M., M. Berenguer, and I. Zawadzki, 2010: The diurnal cycle of precipitation from continental radar mosaics and numerical weather prediction models. Part I:

Methodology and seasonal comparison. *Monthly Weather Review*, **138,** 3084–3106.

Torres-Alavez, A., T. Cavazos, and C. Turrent, 2014: Land–sea thermal contrast and intensity of the North American monsoon under climate change conditions. *Journal of Climate*, **27,** 4566–4580.

Trier, S. B., and D. B. Parsons, 1993: Evolution of environmental conditions preceding the development of a nocturnal mesoscale convective complex. *Monthly Weather Review*, **121,** 1078–1098.

Trier, S. B., J. W. Wilson, D. A. Ahijevych, and R. A. Sobash, 2017: Mesoscale vertical motions near nocturnal convection initiation in PECAN. *Monthly Weather Review*, **145,** 2919–2941.

Trenberth, K. E., A. Dai, R. M. Rasmussen, and D. B. Parsons, 2003: The changing character of precipitation. *Bulletin of the American Meteorological Society*, **84,** 1205–1217.

Tulich, S. N., G. N. Kiladis, and A. Suzuki-Parker, 2011: Convectively coupled Kelvin and easterly waves in a regional climate simulation of the tropics. *Climate Dynamics*, **36,** 185–203.

Tuttle, J. D., and C. A. Davis, 2006: Corridors of warm season precipitation in the central United States. *Monthly Weather Review*, **134,** 2297–2317.

Van Den Broeke, M. S., A. Kalin, J. A. Torres-Alavez, R. Oglesby, and Q. Hu, 2017: A warm-season comparison of WRF coupled to the CLM4.0, Noah-MP, and bucket hydrology land surface schemes over the central United States. Submitted to *Theoretical and Applied Climatology*.

Wallace, J. M., 1975: Diurnal variations in precipitation and thunderstorm frequency over the conterminous United States. *Monthly Weather Review*, **103,** 406–419.

Wang, B., and H. Yang, 2008: Hydrological issues in lateral boundary conditions for regional climate modeling: Simulation of East Asian summer monsoon in 1998. *Climate Dynamics*, **31,** 477–490.

Wang, S.-Y., and T.-C. Chen, 2009: The late-spring maximum of rainfall over the U.S. Central Plains and the role of the low-level jet. *Journal of Climate*, **22,** 4696–4709.

Weaver, S.J. and S. Nigam, 2008: Variability of the Great Plains low-level jet: Large-scale circulation context and hydroclimate impacts. *Journal of Climate*, **21,** 1532–1551.

Weisman, M. L., W. C. Skamarock, and J. B. Klemp, 1997: The resolution dependence of explicitly modeled convective systems. *Monthly Weather Review*, **125,** 527–548.

Wexler, H., 1961: A boundary-layer interpretation of the low-level jet. *Tellus*, **13,** 368–378.

Whiteman, C. D., X. Bian, and S. Zhong, 1997: Low-level jet climatology from enhanced rawinsonde observations at a site in the southern Great Plains. *Journal of Applied Meteorology*, **36,** 1363–1376.

Wilson, J.W., and R. D. Roberts, 2006: Summary of convective storm initiation and evolution during IHOP: Observational and modeling perspective. *Monthly Weather Review*, **134,** 23–47.

Xie, S. and M. Zhang, 2000: Impact of the convection trigger function on single-column model simulations. *Journal of Geophysical Research: Atmospheres*, **105,** 14983–14996.

Zhang, C., Y. Wang, and K. Hamilton, 2011: Improved representation of boundary layer clouds over the southeast Pacific in ARW-WRF using a modified Tiedtke cumulus parameterization scheme. *Monthly Weather Review*, **139,** 3489–3513.

Zhang, G. J., 2003: Roles of tropospheric and boundary layer forcing in the diurnal cycle of convection in the U.S. southern Great Plains. *Geophysical Research Letters*, **30,** 2281.

Zhang, Y., V. Dulière, P. W. Mote, and E. P. Salathé Jr., 2009: Evaluation of WRF and HadRM mesoscale climate simulations over the U.S. Pacific Northwest. *Journal of Climate*, **22,** 5511–5526.

Zheng, Y., K. Alapaty, J. A. Herwehe, A. D. Del Genio, and D. Niyogi, 2016: Improving high-resolution weather forecasts using the Weather Research and Forecasting (WRF) Model with an updated Kain–Fritsch scheme. *Monthly Weather Review*, **144,** 833–860.

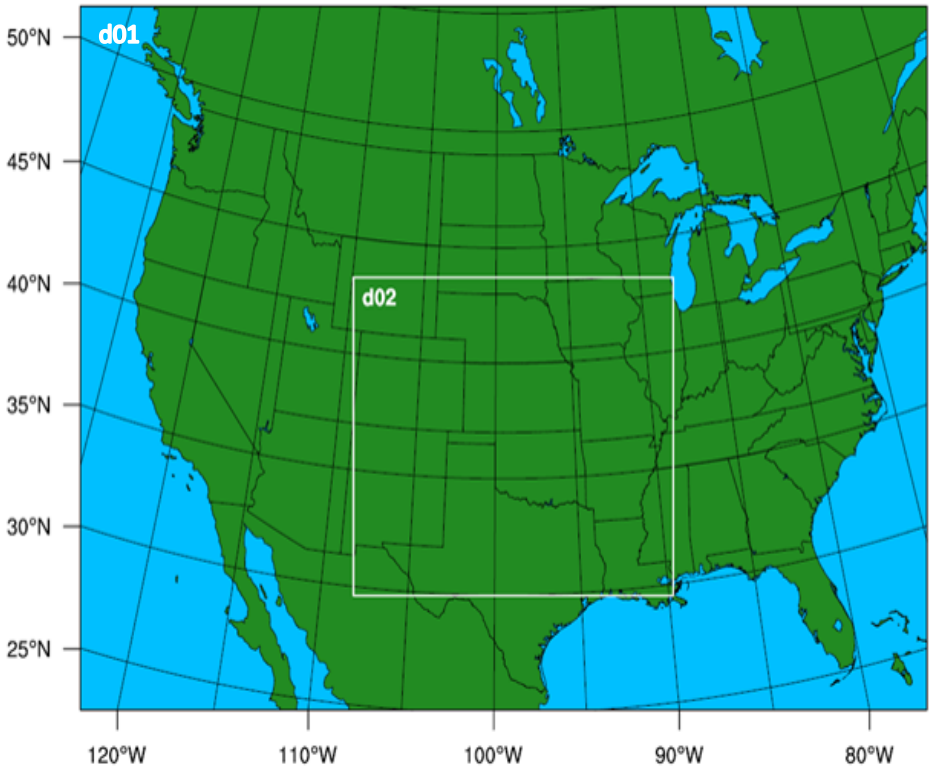

Figure 1. WRF model domains

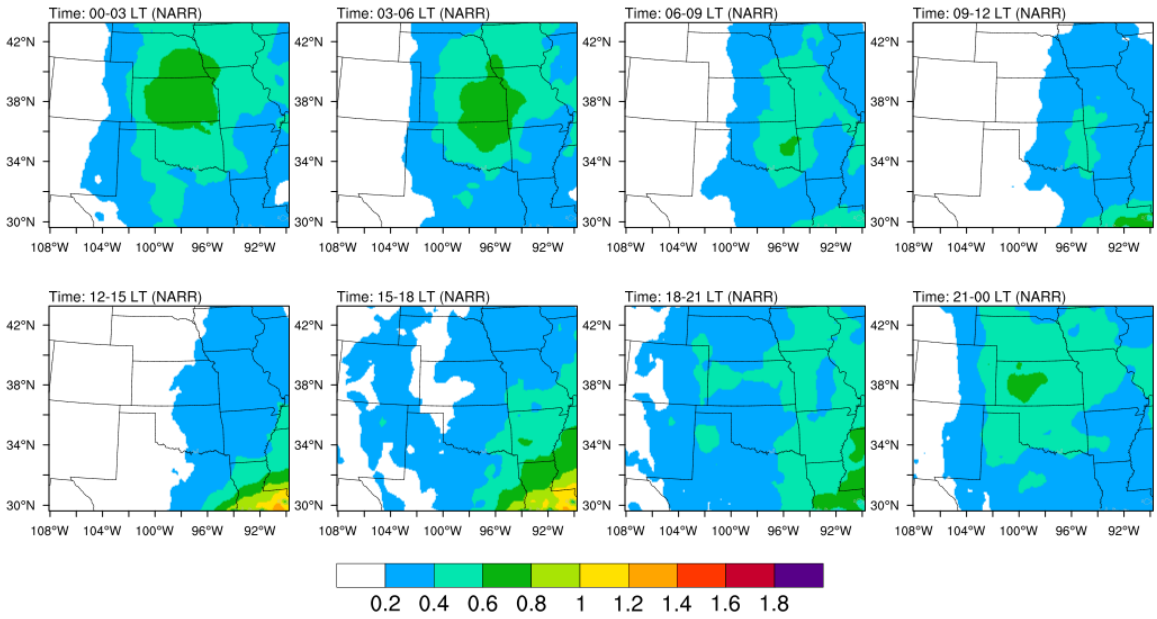

Figure 2. Diurnal cycle of convective precipitation by the NARR data averaged for May, June and July of the 10 years (1991–2000) (unit: mm/3h). The time is given as local time (LT).

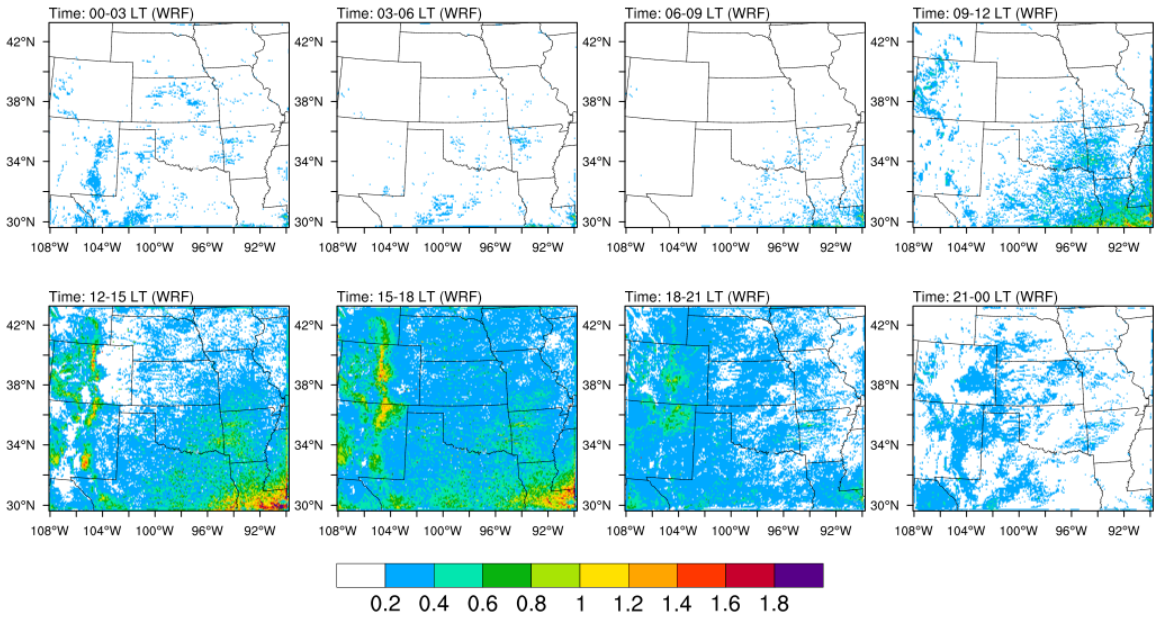

Figure 3. As in Fig. 2 but for the WRF model.

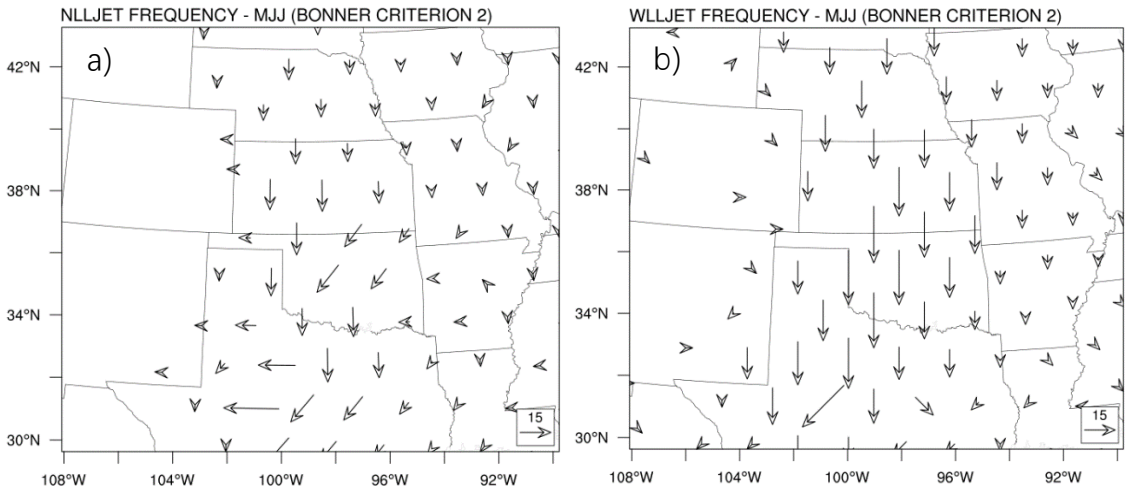

Figure 4. Amplitude and phase of the maximum LLJ frequency, (left) calculated by the NARR data based on Bonner criterion 2 (a), and (right) same as the left but for the WRF model (b). Southward, westward, northward, and eastward vectors indicate maximum frequency at 0000, 0600, 1200, and 1800 local time (LT).

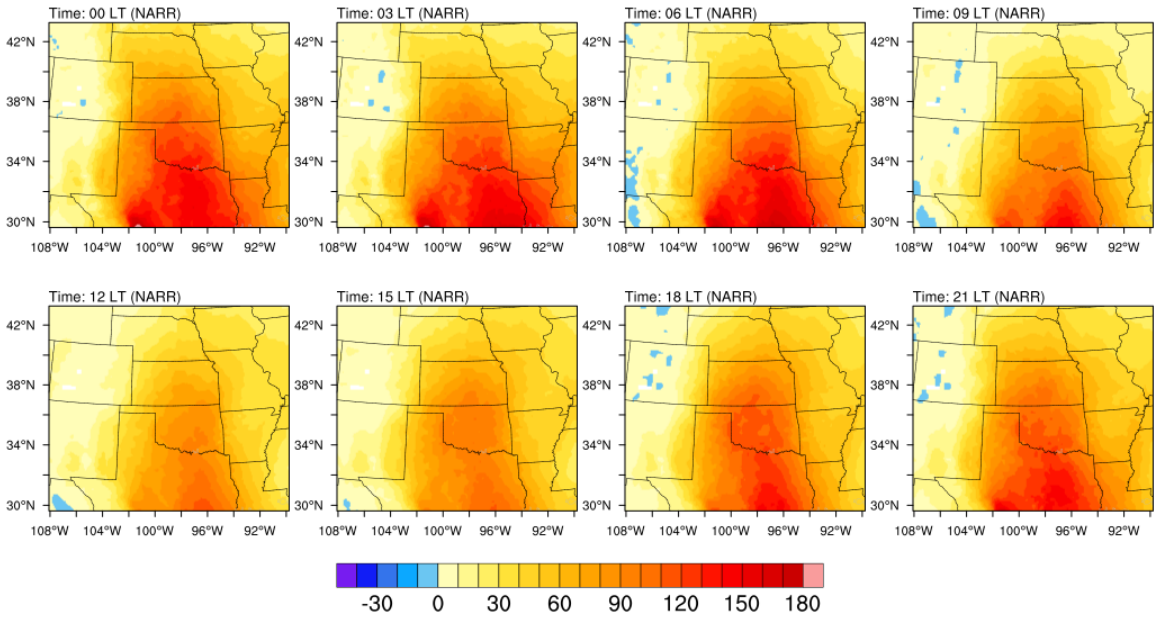

Figure 5. Diurnal cycle of low-level VIMF by the NARR data averaged for May, June and July over the 10 years (1991–2000) (unit: $kg\ m^{-1}\ s^{-1}$). The time is given as local time (LT).

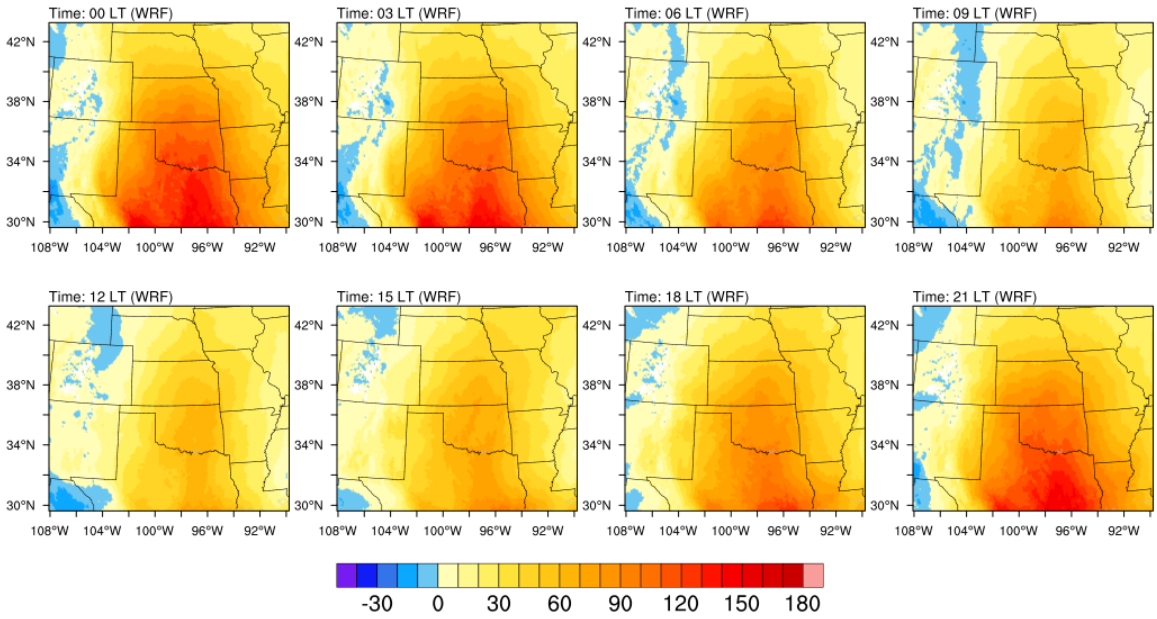

Figure 6. As in Fig. 5 but for the WRF model.

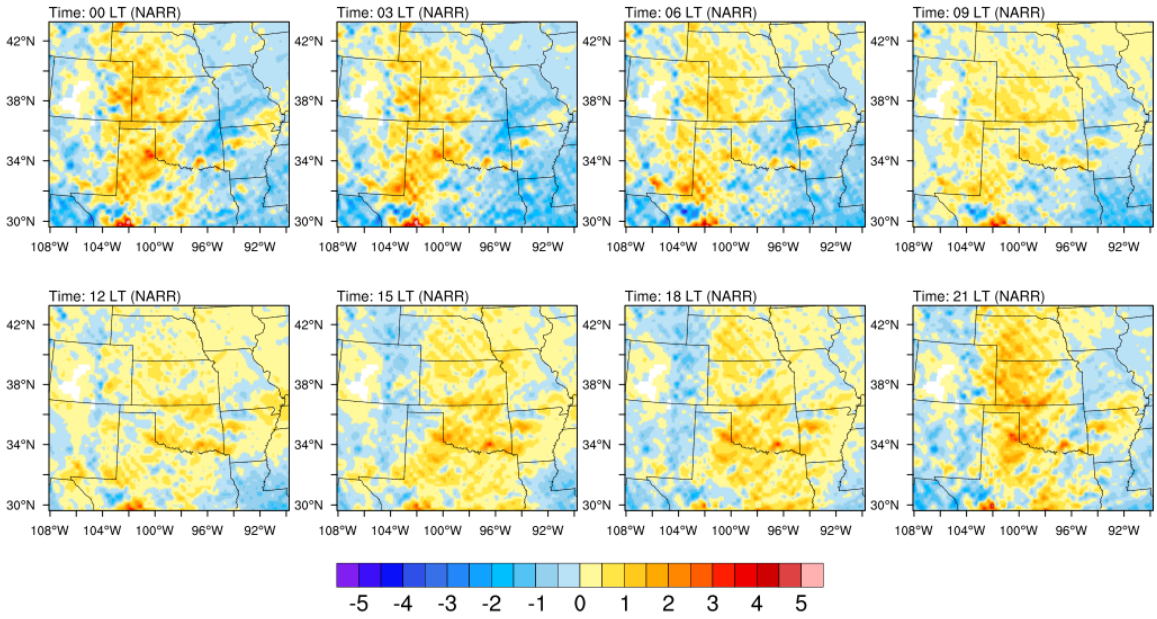

Figure 7. Diurnal cycle of low-level VIMFD by the NARR data averaged for May, June and July over the 10 years (1991–2000) (unit: $10^{-4} kg\ m^{-2}\ s^{-1}$). The time is given as local time (LT).

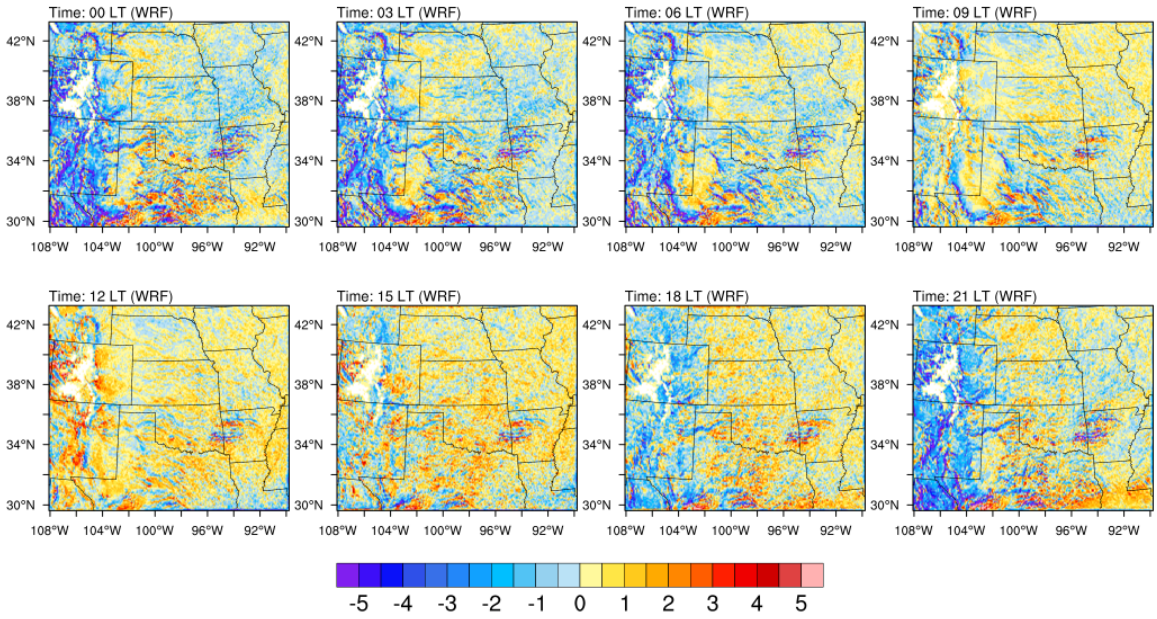

Figure 8. As in Fig. 7 but for the WRF model.

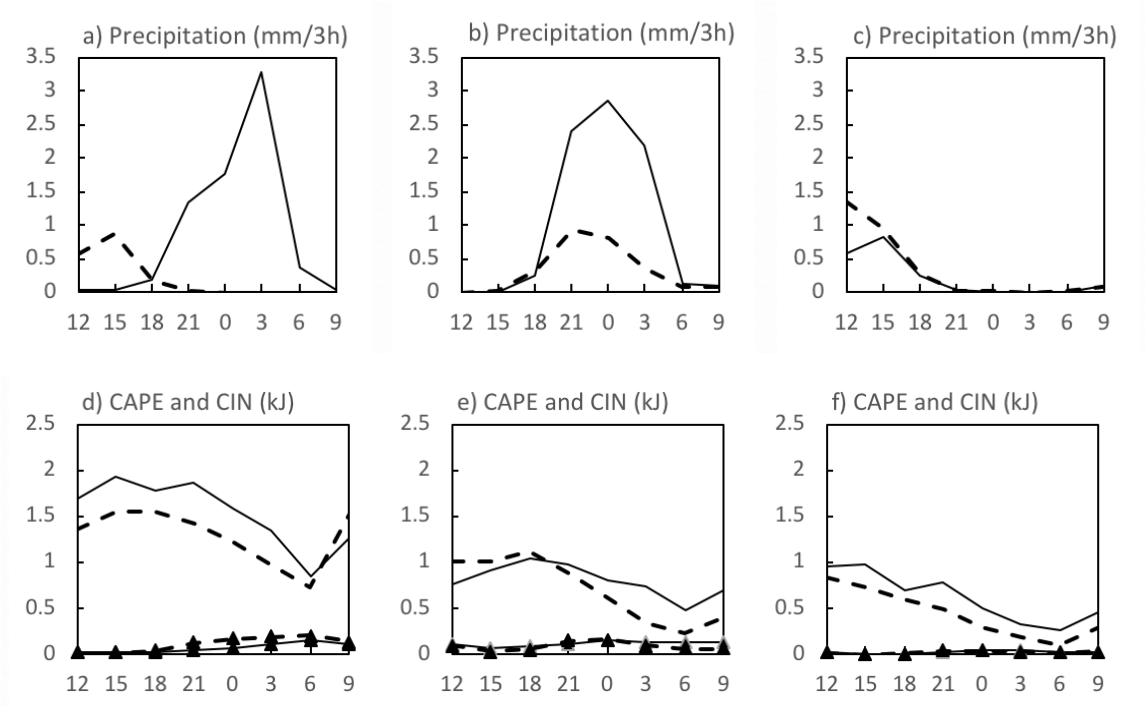

Figure 9. Composite diurnal cycles of the three groups. (left) Group 1, (middle) Group 2, and (right) Group 3: (a)–(c) convective precipitation of the NARR reanalysis (solid) and the WRF model (dashed); (d)–(e) CAPE of the NARR reanalysis (solid) and the WRF model (dashed), and CIN of the NARR reanalysis (solid with markers) and the WRF model (dashed with markers). The time is given as local time (LT).

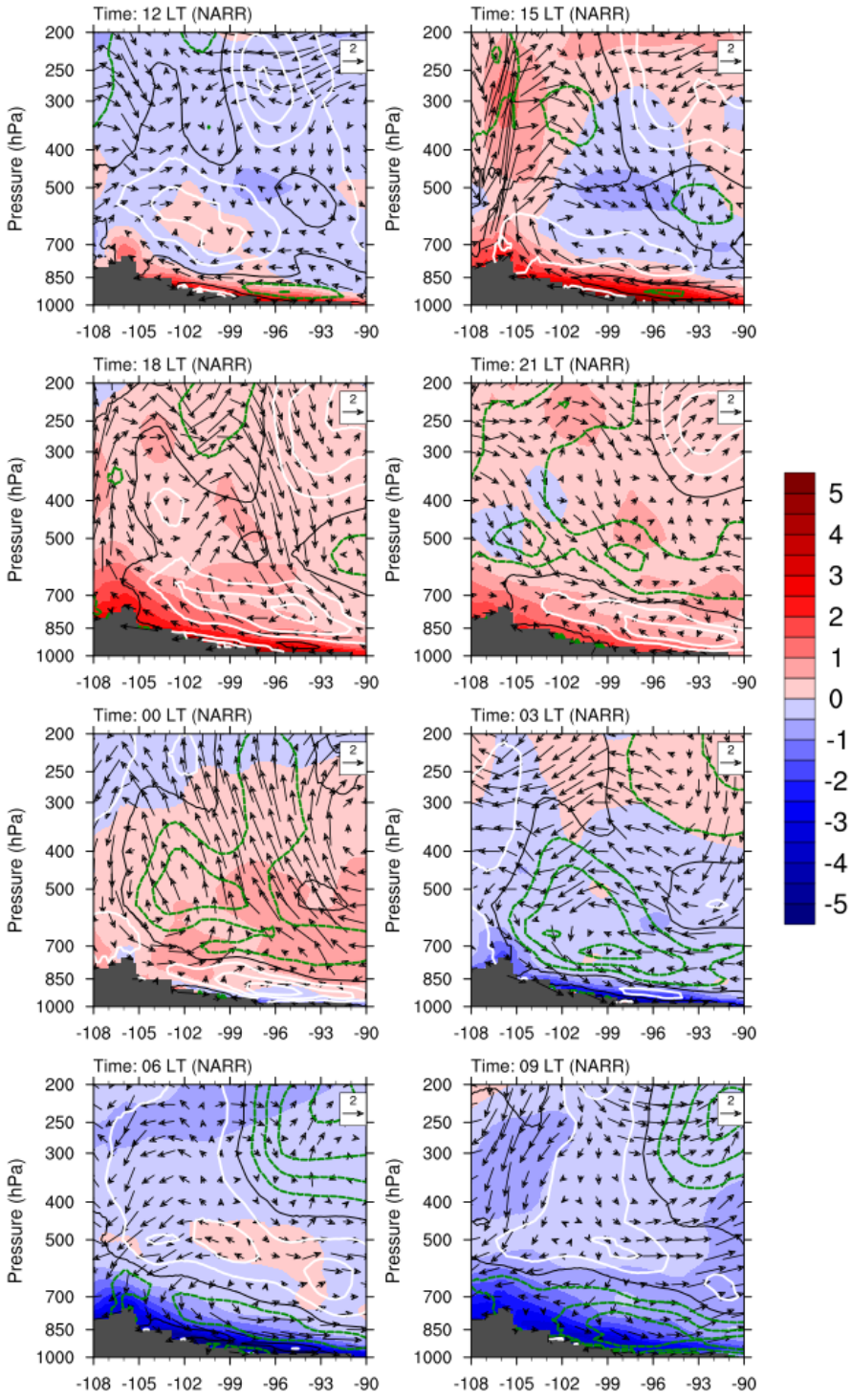

Figure 10. East-west-oriented cross sections of diurnal anomalies (from daily mean) of zonal vertical circulation (u unit: $m\ s^{-1}$, w unit: $cm\ s^{-1}$), temperature (shaded, unit: °C), and meridional wind (contours, intervals of 1 $m\ s^{-1}$) averaged between 37°N and 39°N based on the averages of the 10-day composite from the NARR data in the Group 1. The green, black, and white contours are negative, zero and positive anomalies, respectively. The time is given as local time (LT).

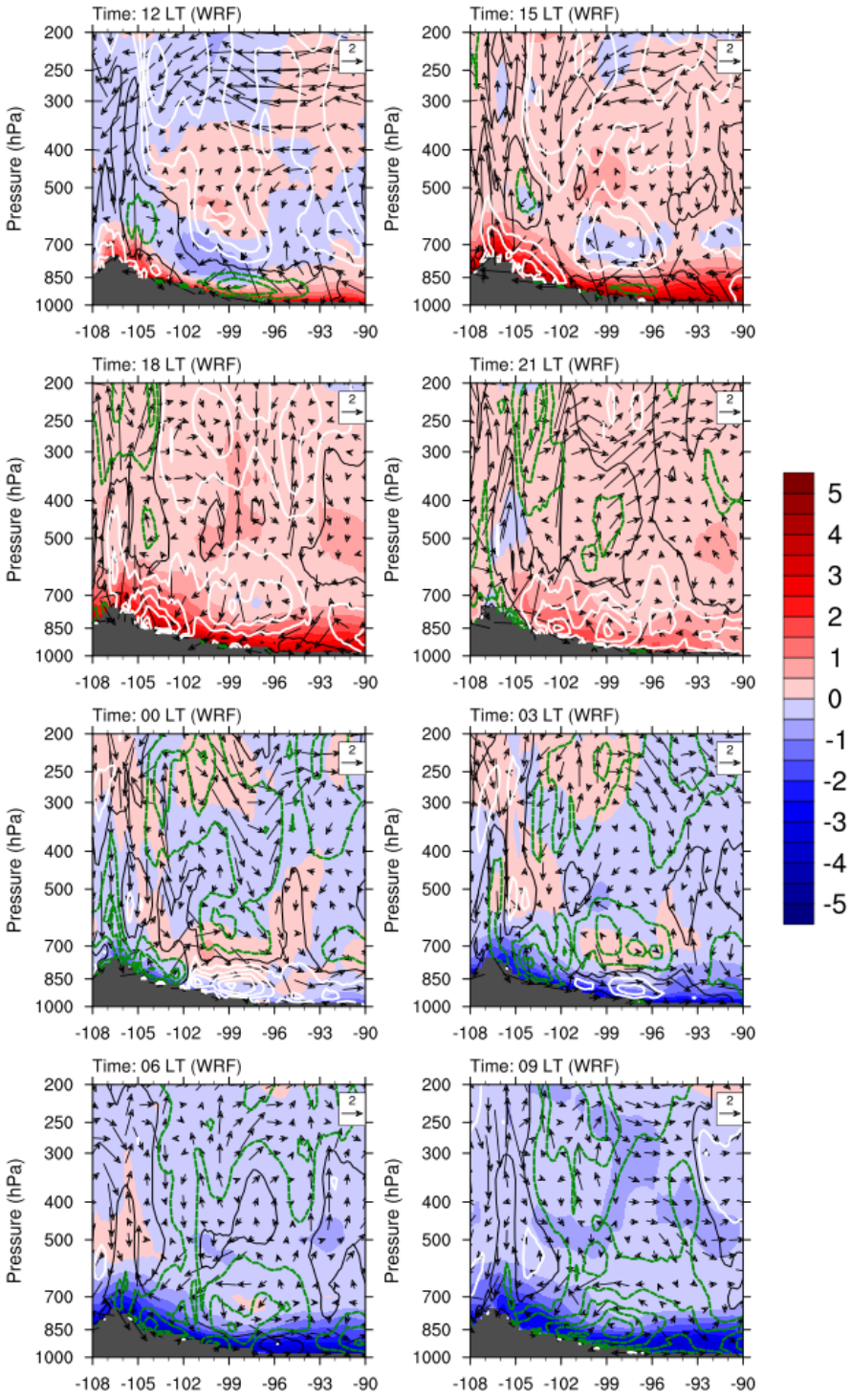

Figure 11. As in Fig. 10 but for the WRF model in the Group 1.

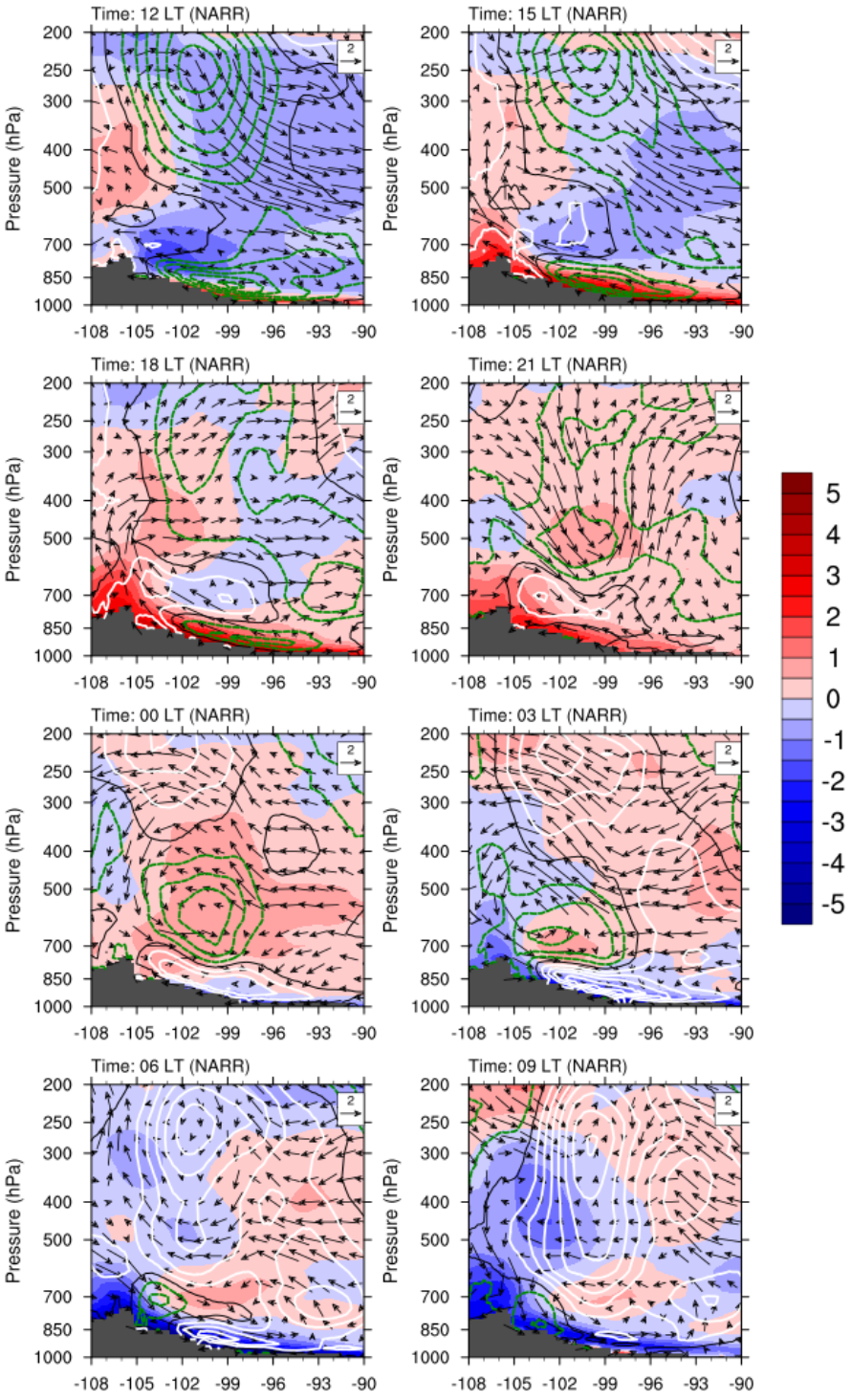

Figure 12. As in Fig. 10 but for the NARR model in the Group 2.

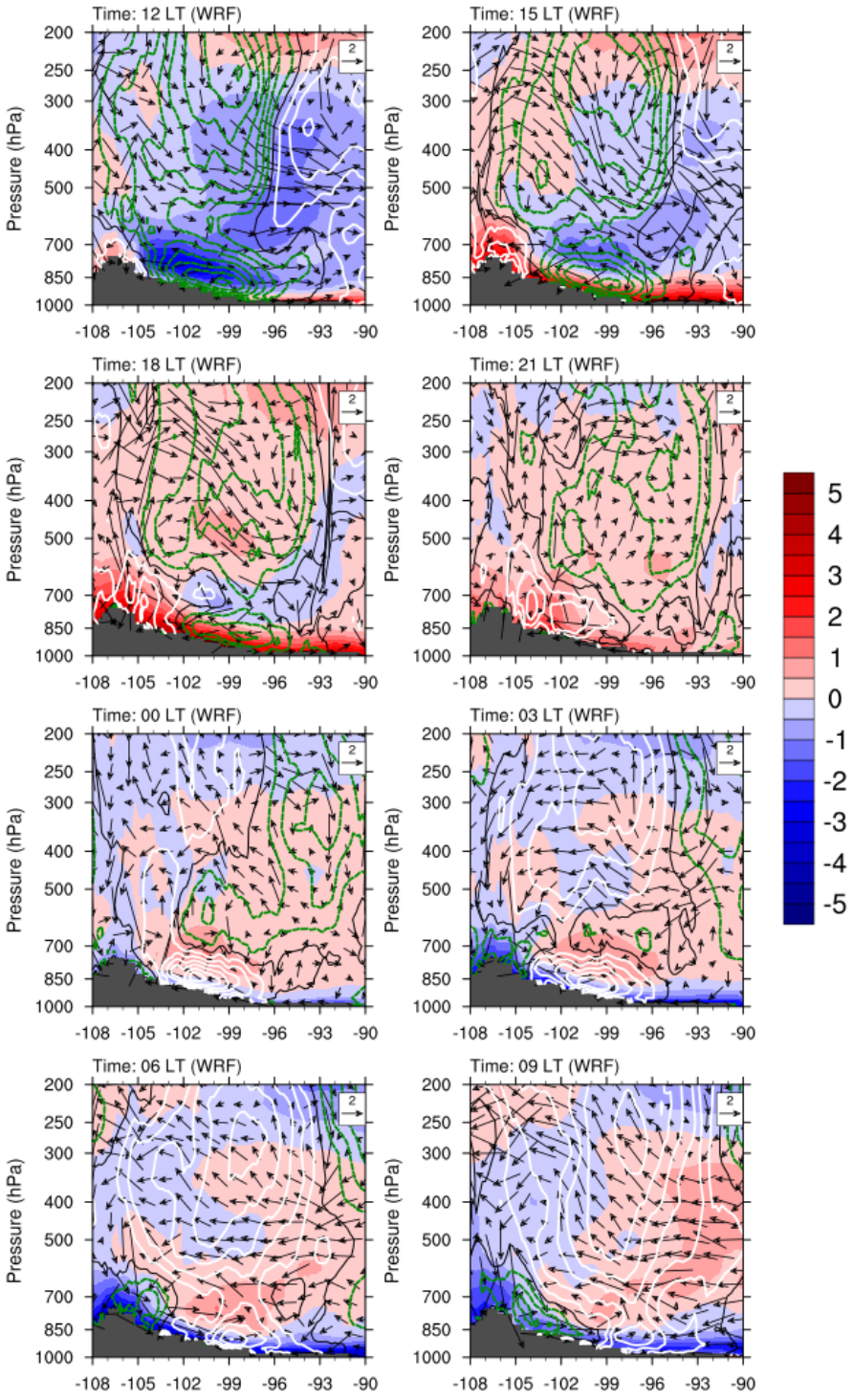

Figure 13. As in Fig. 10 but for the WRF model in the Group 2.

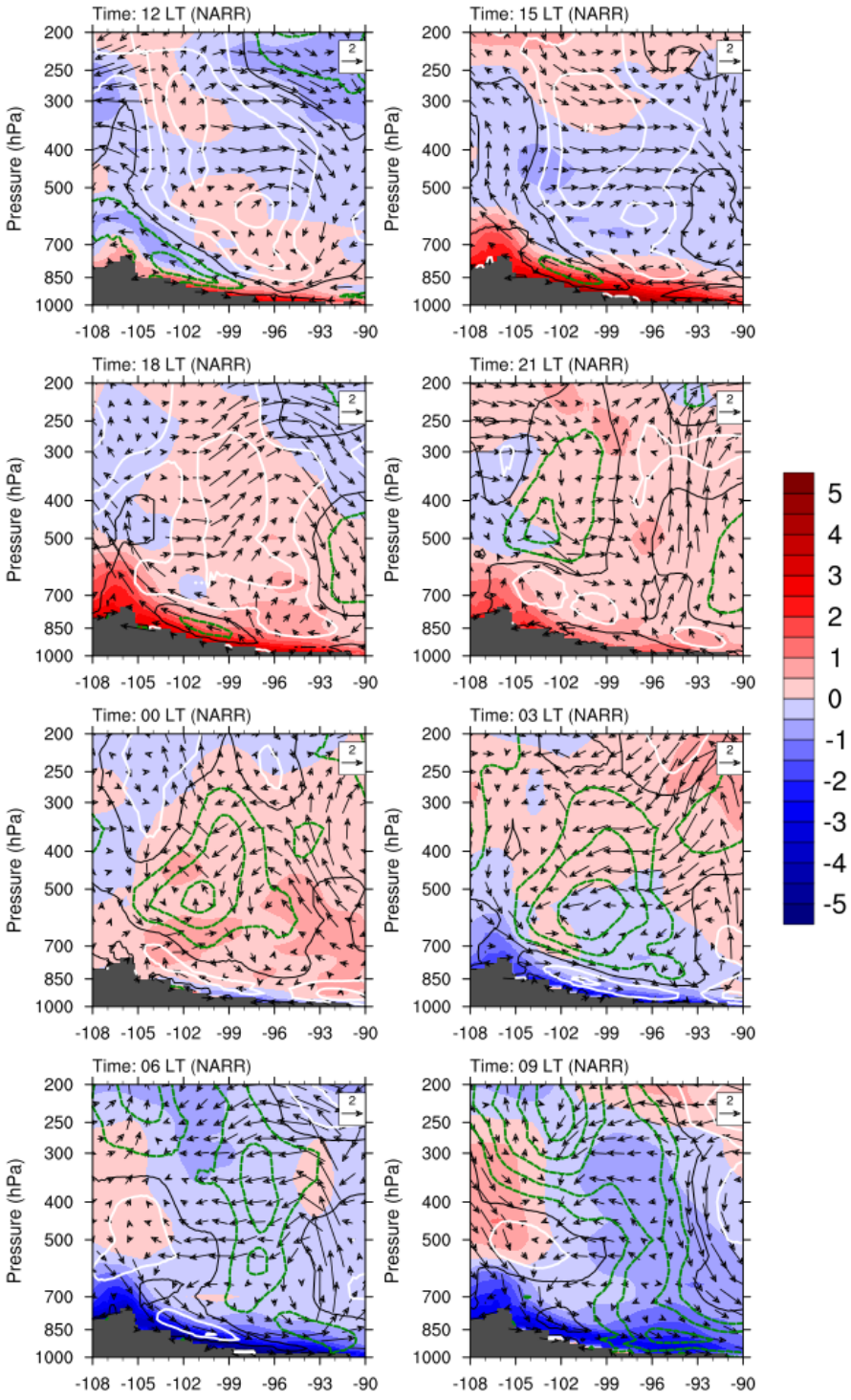

Figure 14. As in Fig. 10 but for the NARR model in the Group 3.

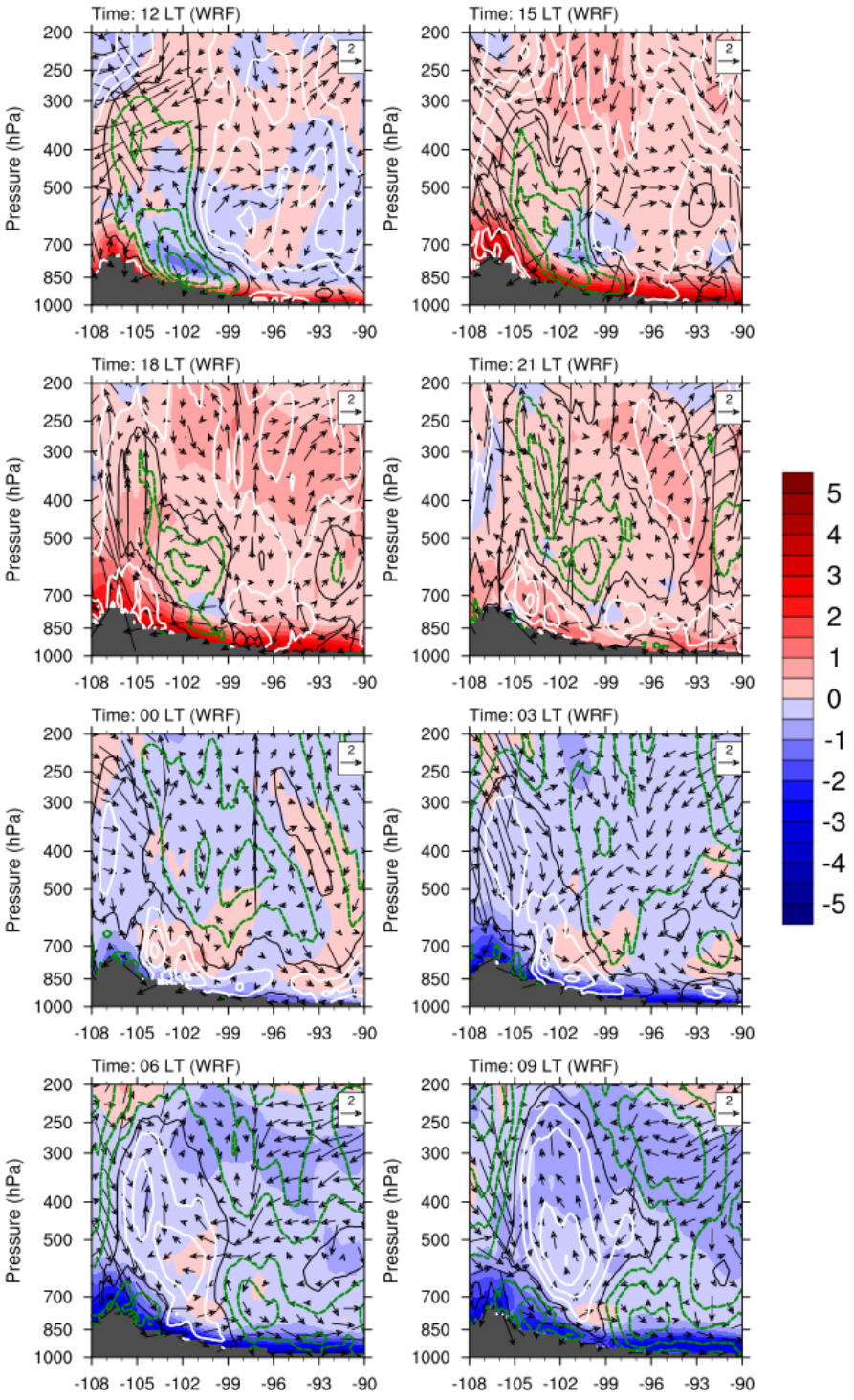

Figure 15. As in Fig. 10 but for the WRF model in the Group 3.

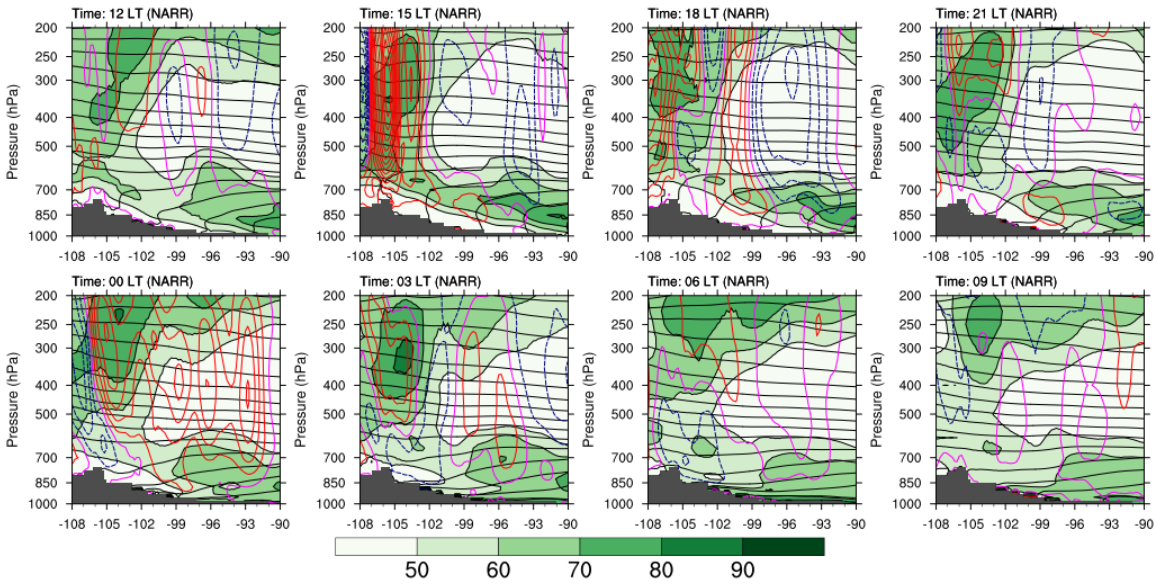

Figure 16. East-west-oriented cross sections of diurnal cycles of vertical velocity (colored contours, intervals of 1 $cm\ s^{-1}$), relative humidity (green shaded, unit: %) and isentropes (black contours, intervals of 3K) averaged between 37°N and 39°N based on the averages of the 10-day composite from the NARR data in the Group 1. The red, purple, and blue contours represent positive, zero and negative velocities, respectively. The time is given as local time (LT).

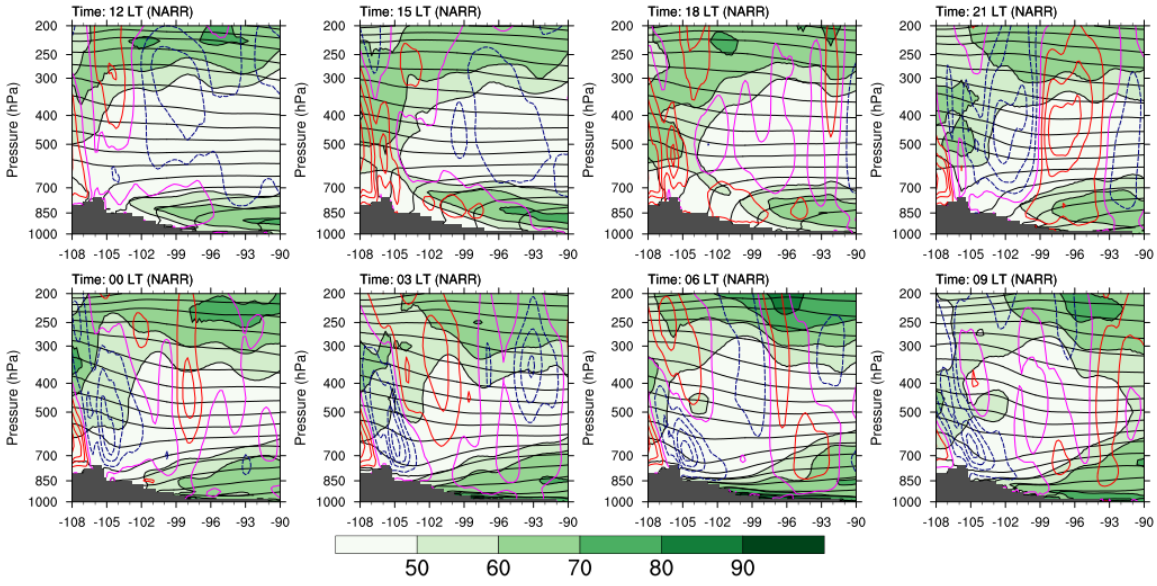

Figure 17. As in Fig. 16 but for Group 2.

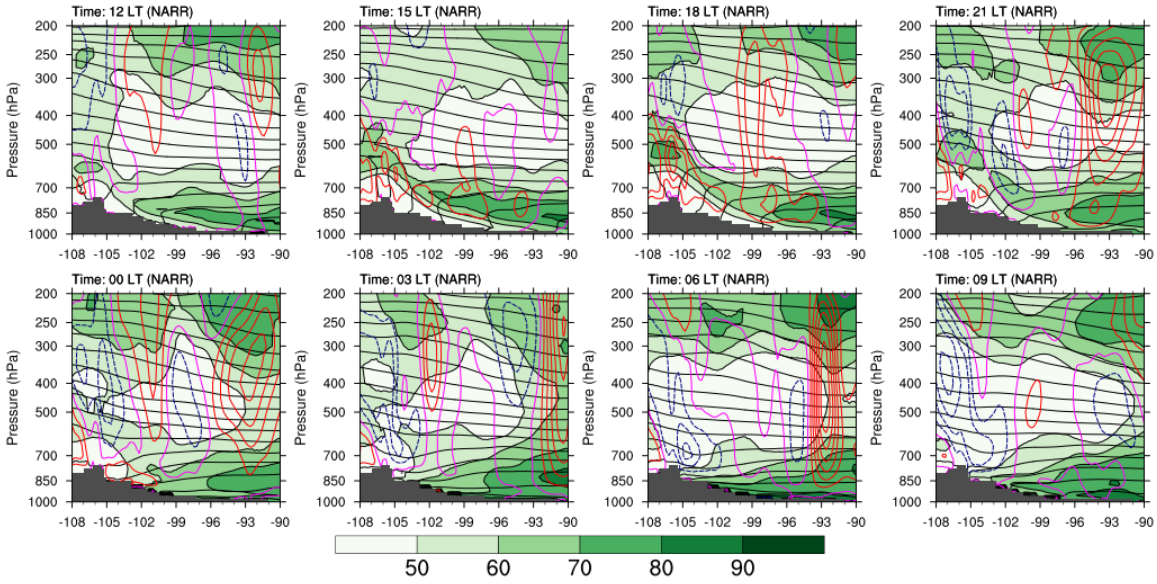

Figure 18. As in Fig. 16 but for Group 3.

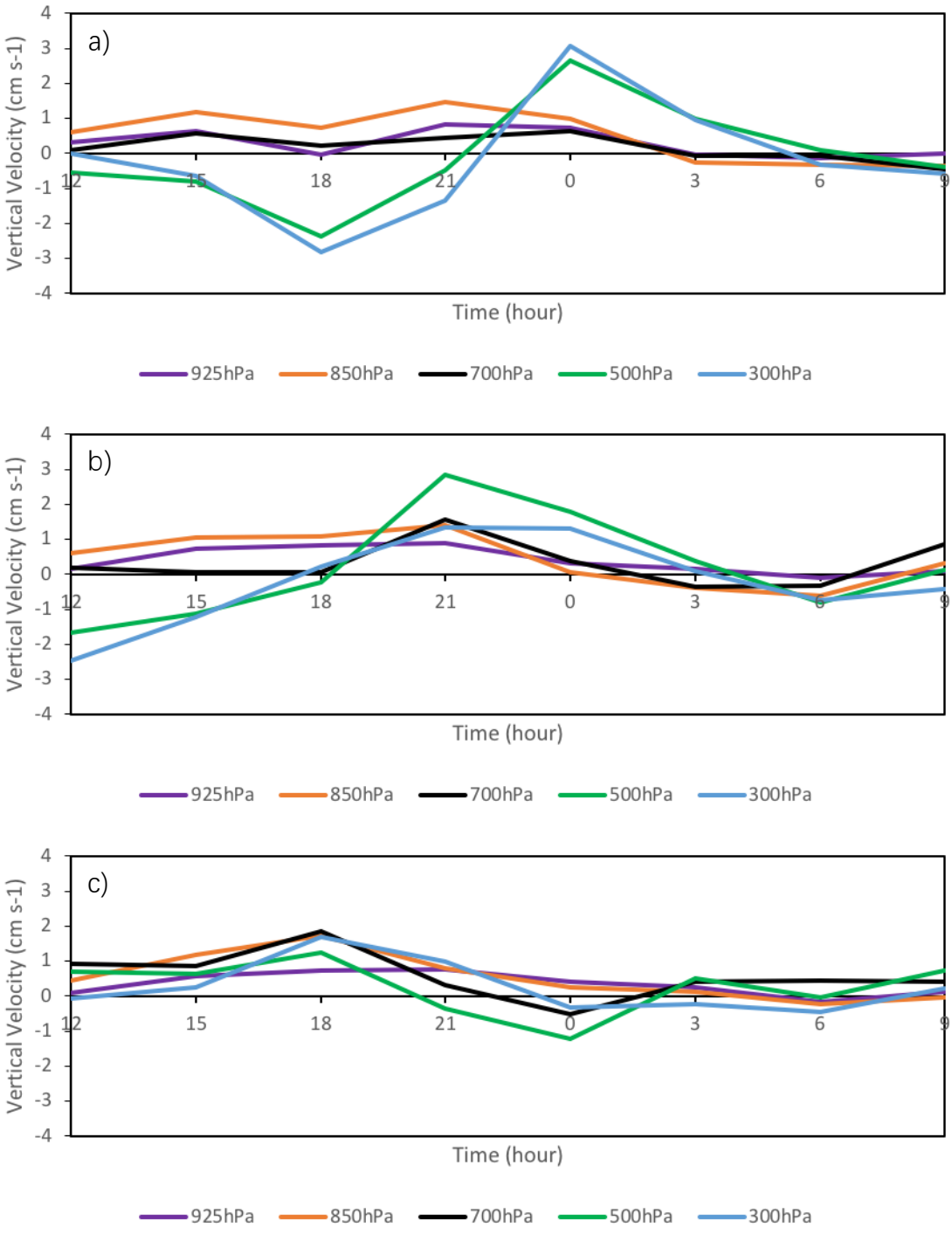

Figure 19. Diurnal cycles of vertical velocity (unit: $cm\ s^{-1}$) over the composite area, southern Kansas (37-39˚N, 99-97˚W), for (a) Group 1, (b) Group 2, and (c) Group 3. The time is given as local time (LT).